Optimisation of arrays of flap-type oscillating wave surge converters

I.F. Noad[1] and R. Porter

School of Mathematics, University Walk, Bristol, BS8 1TW, UK

Abstract

In this paper a finite array of hinged flap-type wave energy converters are modelled using a mathematical approach. These are illustrative of the Oyster device of Aquamarine Power LTD[2]. A novel semi-analytic solution method is presented for a set of boundary-value problems involving the scattering and radiation of waves by thin barriers used to model the device hydrodynamics. The approach makes use of the geometry to apply Fourier transforms, deriving non-singular integral equations in terms of the jumps in pressure across the flaps. These are then solved numerically using a highly efficient Galerkin expansion method. The focus of the results is on optimisation. We suggest optimal parameters for a single device, highlighting key features of its success and identifying flap length as crucial to device performance. This optimisation is then carried through to arrays with optimal arrangements and spacings being determined for a model sea state. Here, the lateral displacement of the devices emerges as a critical factor in optimal array configuration.

1. Introduction

The development of technology for the conversion of ocean wave energy into a source of useable energy has been a long and slow process. Interest in the potential of wave energy converters (WECs) as a significant source of renewable energy started in earnest in the mid-1970's. However, the route to full scale commerical deployment has been plagued by a combination of factors, not least the difficulty in engineering devices exposed to the harsh marine climate which are both reliable and efficient. In the UK there are two devices which have recently emerged as promising candidates for large scale commercial success: the Pelamis device manufactured by Ocean Power Delivery and the Oyster device of Aquamarine Power LTD[2]. Although engineering development challenges remain both have enjoyed some success as single device prototypes and the emerging challenge is in extending to multiple devices in a wave farm array.

This paper uses a mathematical approach to consider a variety of aspects concerned with the operation of a hinged flap-type device which is illustrative of the Oyster device referred to above. The Oyster device itself was derived from research carried out at Queens University, Belfast, UK, [see 22, for example] and we follow some of the basic modelling assumptions used in that early work. Thus, we consider a wave energy converter that is assumed to operate in shallow water environments. This is comprised of a long, buoyant, rectangular paddle extending upwards through the water surface. The paddle is hinged along a horizontal axis on a fixed foundation protruding vertically from the sea bed. When waves are incident upon the flap, it pitches about the submerged hinge and power is generated by this pitching motion relative to the fixed foundation. In the hydrodynamic modelling needed for the computation of power output we make a number of assumptions. The first is that the width of the flap-type paddle and its foundation are small enough with respect to typical wavelengths to be regarded as infinitely thin. The next is to assume that linearised wave theory can be employed, an approximation requiring wave steepnesses and paddle pitching angles to be small enough. Such approximations are standard in the analysis of wave energy devices, see Cruz [4] for example.

[1]Corresponding author. Tel.:+44 7892 829 177.
Email addresses: imogen.noad@bristol.ac.uk (I.F. Noad), richard.porter@bristol.ac.uk (R. Porter).

[2]`http://www.aquamarinepower.com/`

To date, much of the development work on Oyster has been carried out using numerical CFD and experimental wave tank testing [22, 9]. However, recently a series of papers, [17, 16, 15] have approached the hinged flap-type problem. Thus, an infinite periodic array, a single device and a finite number of in-line devices have all been considered. Our paper uses the same background theory as contained in [16] and [15]. However, there are some differences which will be alluded to in the description of our approach below.

The main purposes of the present paper are three-fold. First to describe the principle of operation of a single flap-type device. There are good reasons to suppose that high performance is unlikely. In particular, it is well known that for fore-aft symmetric devices designed to operate in a single mode of motion (pitch in the case of the Oyster) efficiencies are limited to a maximum of 50% in a two-dimensional setting (corresponding here to a flap extending across a finite-width wave tank). Other device concepts such as the Bristol Cylinder [5] and the Salter Duck [18] which are designed to operate in a more complicated manner are theoretically capable of efficiencies up to 100%. Moreover, hinged flap-type converters representative of Oyster are known to have a natural resonant period of about 20s [22] well beyond the range of energy-dense periods in a real sea spectrum. We will be able to describe why the hinged flap-type WEC of finite length works better than suggested by these two counter arguments. This insight is not contained in the paper of Renzi and Dias [16].

The second main purpose of the paper is to demonstrate a mathematical solution method to the hydrodynamic problems that arise when considering a finite array of N flap-type devices which are parallel but otherwise positioned arbitrarily. Thus is it shown how an application of Fourier transforms leads to N coupled integral equations in terms of N unknown functions relating to jumps in hydrodynamic pressures across the flaps. Furthermore, application of a Galerkin approximation involving a judicious choice of expansion functions reduces the integral equations to a low-order system of equations whose solutions are efficiently and accurately computed. This approach is different to Renzi and Dias [16], Renzi et al. [15] who used Green's functions to develop hypersingular integral equations, solved by collocation.

The third purpose is to exploit the numerical efficiency of solutions for arrays of devices to perform an optimisation over a number of free parameters associated with the theoretical problem. This allows us, in the first instance, to assess the optimal configuration of a single flap device under a realistic random sea state. In particular, it is demonstrated that the length of the flap is critical to its performance. Continuing further, the configuration of a multi-flap array is considered, the optimisation procedure being used to select the arrangement of the array which yields the highest total power output, again in a model sea state. Here, the stagger and distances between elements of the array emerge as critical factors in determining array performance.

One of the difficulties in designing arrays of devices – and the reason why we have resorted to using numerical optimisation in this paper – is that there are limited theoretical results for optimisation of power from multiple elements of an array. This is in stark contrast to what is known about how single devices work and are optimised. In the Appendix we have provided a series of results relating to optimal power for arrays of devices under practical constraints on the power take-off. It is hard to imagine that all of these results are new, although the authors have been unable to find them in the literature – perhaps because they have limited application. However, for an array of two identical devices new results of practical use have been derived for the maximisation of power.

In §2 of the paper we derive expressions for the power absorption and relate them to certain properties of scattering and radiation potentials satisfying linear water wave problems and associated with the scattering and radiation of waves by each of the thin barriers. Much of this section is guided by principles of wave power conversion calculations set out, for example, in Thomas [20]. These are then extended in the Appendix where strategies are developed for determining optimal mechanical damping for practical power take-off systems in the context of an array and new results are derived. We go on to specify the hydrodynamic problems associated with the scattering and radiation of waves by a finite array of parallel flaps in §3 and in §4 a new integral equation formulation is derived and presented for their approximate solution.

Certain elements which are key to the numerical calculations and accuracy of the subsequent approximate solutions are discussed in §5. It is here that we introduce a self-similar spectrum applicable to the near-shore context and used in the determination of the mean capture factor.

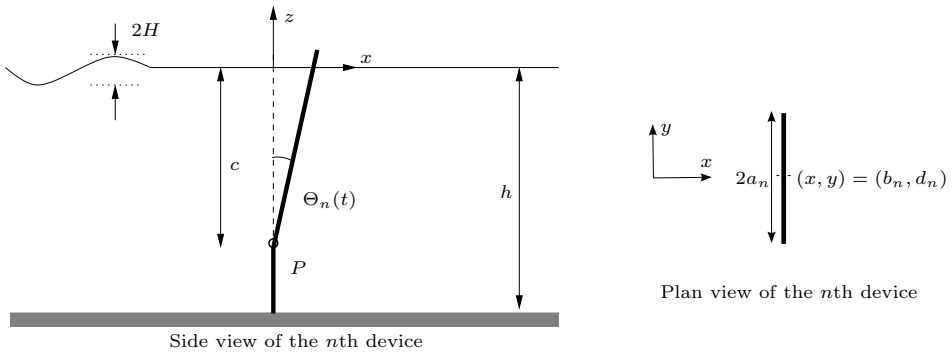

Figure 1: Some key parameters imposed on side and plan views of the nth flap converter used in the hydrodynamic model.

This is employed throughout the results as a measure for optimal performance in random waves representative of a real sea. Results are then presented in §6; initially for a single device and then, with increasing generality, for arrays of 2,3 and 5 devices. Finally, in §7 conclusions are drawn and suggestions for future work are given.

In the final preparation for submission of this paper the authors became aware of a recently published paper, Sarkar et al. [19] which considers the same problem of power take-off from arbitrary arrays of parallel flap-type devices. There are, of course, inevitable similarities between the paper of Sarkar et al. [19] and the present paper. Thus, the hydrodynamical modelling and model assumptions are the same and the focus on assessing the performance differences between in-line and staggered arrays is similar. Some of the conclusions are similar too. However, there are some significant differences in the two pieces of work. The features of our paper highlighted earlier in the Introduction, such as the mathematical analysis of the single device performance and the development of analytic expressions for optimising power for arrays, are new. In terms of the approach taken to solve the hydrodynamic problem, Sarkar et al. [19] use Green's functions to develop hypersingular integral equations numerically approximated by collocation methods. In constrast, we have taken a very different mathematical approach, using Fourier transforms to develop non-singular integral equations which are numerically approximated by Galerkin's method. This difference is significant in terms of numerical efficiency of computations. Numerical simulations on a test problem performed by Sarkar et al. [19] on a 3.4Ghz PC with 16GB of RAM are quoted as taking 6 minutes on average (page 7). On a similar piece of equipment (a 3.0Ghz PC with 16GB RAM) our method applied to their same problem is roughly 20 times faster. This increase in numerical efficiency is crucial if one wants to implement optimisation methods as we have done here.

Finally, the focus of the numerical results is very different here to Sarkar et al. [19] where the main focus is on q-factors for central device elements as functions of wave period. There, discrete configurations of elements in the array have been considered with fixed spacings and mainly in normally-incident waves. We have instead focused on the total power developed by the whole array under a random wave spectrum (adjusted for the nearshore environment) with directional spreading and, instead of fixed spacings, we have implemented an optimisation routine which selects the optimal array configuration. Some of the conclusions made by Sarkar et al. [19] we agree with, such as general rules preferring certain types of stagger over others. However, the results presented here have been able to select optimal configurations at spacings well beyond those considered in Sarkar et al. [19].

2. Formulation

Cartesian coordinates have been chosen with the origin at the mean free surface level and z pointing vertically upwards. The fluid has density ρ and is of constant, finite depth h. We consider a finite array of N flap-type devices, each labelled by the index n. These are oriented parallel to the y-axis, have length denoted by $2a_n$ and are centred (when viewed from above) at

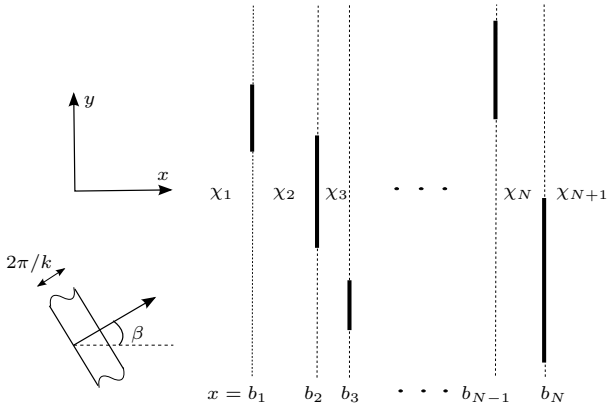

Figure 2: Some key parameters imposed on a plan view of an example configuration of an array of flap converters.

the points $(x, y) = (b_n, d_n)$ such that $b_1 \leq b_2 \leq ... \leq b_N$. The hydrodynamic model assumes the flaps are infinitely thin and buoyant so that when at rest they occupy the vertical planes $\{x = b_n, d_n - a_n < y < d_n + a_n, -h < z < 0\}$ for $n = 1, ..., N$. They are hinged along horizontal axes $(x, z) = (b_n, -c)$, which are denoted in figure 1 by P. Above its pivot each flap is free to move and below it is held fixed and vertical. $\Theta_n(t)$ is the (assumed small) angle through which the nth flap has rotated measured anticlockwise from the vertical. A standard small-amplitude, linearised theory of water waves is used. A monochromatic wave of assumed small amplitude $H/2$ and radian frequency ω is incident on the array from $x < 0$ making an anti-clockwise angle β with the positive x-direction where $\beta \in (-\pi/2, \pi/2)$.

The time-dependent problem is as follows. We define a velocity potential $\Phi(x, y, z, t)$ satisfying

$$\bigtriangledown^2 \Phi = 0, \qquad \text{in the fluid} \tag{2.1}$$

with linearised dynamic and kinematic free surface conditions

$$\Phi_t + g\zeta = 0, \qquad \text{and} \qquad \zeta_t = \Phi_z, \qquad \text{on } z = 0 \tag{2.2}$$

where $\zeta(x, y, t)$ denotes the free surface and g is the gravitational acceleration. On the bottom of the fluid,

$$\Phi_z = 0, \qquad \text{on } z = -h. \tag{2.3}$$

Having considered the boundary conditions on the free surface and sea bed we now turn our attention to the boundaries formed by the flaps themselves. On the nth flap, the time-dependent linearised kinematic condition is

$$\Phi_x \left(b_n^{\pm}, y, z, t\right) = \dot{\Theta}_n(t)\, u(z), \qquad \text{where} \qquad u(z) = \begin{cases} 0, & -h < z < -c \\ z + c, & -c < z < 0 \end{cases} \tag{2.4}$$

for $y \in (d_n - a_n, d_n + a_n)$ and $n = 1, ..., N$.

Now, since we are interested in the flaps' capacity for wave energy absorption we must consider the forces which are acting. Applying Newton's second law for rotation to the motion of each of the N flaps about their pivots (which occupy a horizontal axes given by $(x, z) = (b_n, -c)$ for $d_n - a_n < y < d_n + a_n$) gives

$$I_n \ddot{\Theta}_n(t) = -C_n \Theta_n(t) + X_{w,n}(t) + X_{e,n}(t), \qquad \text{for } n = 1, ..., N, \tag{2.5}$$

where I_n denotes the moment of inertia and C_n the restoring moment (produced by assumed buoyancy) of the nth flap about its pivot. The values of these quantities are determined by the physical properties of the corresponding flaps, namely their dimensions and density. Further, $X_{w,n}$ are the time-dependent wave torques acting on each of the N flaps, given by the integrated

moment of the pressure forces acting on the nth flap in the positive x-direction:

$$X_{w,n}(t) = \rho \int_{d_n - a_n}^{d_n + a_n} \int_{-h}^{0} [\Phi_t\left(b_n^+, y, z, t\right) - \Phi_t\left(b_n^-, y, z, t\right)] u(z)\, dz\, dy \qquad \text{for } n = 1, ..., N. \tag{2.6}$$

Finally, $X_{e,n}$ denote the external mechanical torques produced by the power take-off on each of the N flaps.

Now, with the formulation of the time-dependent problem set out it is convenient to factor out the assumed harmonic time dependence due to the incident wave by writing

$$\begin{aligned} \Phi(x, y, z, t) &= Re\left\{\phi(x, y, z)\, e^{-i\omega t}\right\}, & \zeta(x, y, t) &= Re\left\{\eta(x, y)\, e^{-i\omega t}\right\}, \\ \dot{\Theta}_n(t) &= Re\left\{\Omega_n e^{-i\omega t}\right\}, & X_{w,e}(t) &= Re\left\{F_{w,e} e^{-i\omega t}\right\}. \end{aligned} \tag{2.7}$$

where Ω_n is the complex angular velocity of the nth device. Its use in this context follows the general convention when formulating wave energy problems.

Since Laplace's equation and the boundary conditions for the velocity potential ϕ are linear we may use the principle of superposition to decompose the problem into component parts

$$\phi(x, y, z) = A\phi^S(x, y, z) + \sum_{m=1}^{N} \Omega_m \phi^m(x, y, z) \qquad \text{where} \qquad A = \frac{igH}{2\omega\psi_0(0)} \tag{2.8}$$

where ψ_0 is a normalised depth eigenfunction and will be defined, along with the incident wave, a little later. Here ϕ^S is associated with the scattering of an incident wave of unit amplitude by flaps held fixed vertically with the scaling A ensuring an incident wave height H (peak to trough). Meanwhile, ϕ^m corresponds to the generation of waves by the mth flap when it experiences a prescribed oscillatory motion in otherwise undisturbed waters and all other flaps are held fixed.

Using (2.7) in (2.1) - (2.3), ϕ^S and ϕ^m satisfy

$$\bigtriangledown^2 \phi^S = 0 \qquad \text{and} \qquad \bigtriangledown^2 \phi^m = 0, \qquad \text{for } m = 1, ..., N, \text{ in the fluid} \tag{2.9}$$

with the combined linear kinematic and dynamic free surface condition giving

$$\phi_z^S - \frac{\omega^2}{g}\phi^S = 0 \qquad \text{and} \qquad \phi_z^m - \frac{\omega^2}{g}\phi^m = 0, \qquad \text{for } m = 1, ..., N \text{ on } z = 0 \tag{2.10}$$

and on the bottom of the fluid,

$$\phi_z^S = 0 \qquad \text{and} \qquad \phi_z^m = 0 \qquad \text{for } m = 1, ..., N \text{ on } z = -h. \tag{2.11}$$

Further, from (2.4) the linearised kinematic condition on the nth flap for the scattering problem is given by

$$\phi_x^S\left(b_n^{\pm}, y, z\right) = 0 \qquad \text{for } -h < z < 0 \text{ and } y \in (d_n - a_n, d_n + a_n),\ n = 1, ..., N, \tag{2.12}$$

since the flap is held fixed forming a solid, vertical barrier. For the remaining potentials, ϕ^m, the condition on the nth flap when the mth flap is oscillating is given by

$$\phi_x^m\left(b_n^{\pm}, y, z\right) = u(z)\, \delta_{mn} \qquad \text{for } y \in (d_n - a_n, d_n + a_n),\ n, m = 1, ..., N \tag{2.13}$$

where the angular velocity was factored out in (2.8).

At this point it is pertinent to introduce the incident wave; a solution defined by its time-independent velocity potential is

$$\phi^I(x, y, z) = e^{ik(x\cos\beta - y\sin\beta)}\psi_0(z) \tag{2.14}$$

where k is the positive, real wave number satisfying $\omega^2 = gk \tanh kh$ and $\psi_0(z)$ is a normalised depth eigenfunction associated with the propagating waves defined by

$$\psi_0(z) = N_0^{-1/2} \cosh k(z + h), \qquad N_0 = \frac{1}{2}\left(1 + \frac{\sinh 2kh}{2kh}\right). \tag{2.15}$$

The potentials ϕ^m, $m = 1, ..., N$ and $\phi^D \equiv \phi^S - \phi^I$ describe outgoing waves at large distances from the flap.

Removing the harmonic time-dependence, Newton's law (2.5) may now be written as

$$-i\omega I_n \Omega_n = -\frac{iC_n}{\omega}\Omega_n + F_{w,n} + F_{e,n} \tag{2.16}$$

where $F_{w,n}$ is correspondingly given by

$$F_{w,n} = -i\omega\rho \int_{d_n-a_n}^{d_n+a_n} \int_{-h}^{0} [\phi\left(b_n^+, y, z\right) - \phi\left(b_n^-, y, z\right)]u(z)dzdy. \tag{2.17}$$

Using an analagous decomposition of $F_{w,n}$ to that of ϕ (given in (2.8)) we write

$$F_{w,n} = AF_{S,n} + \sum_{m=1}^{N} \Omega_m F_{m,n} \tag{2.18}$$

where

$$F_{S,n} = -i\omega\rho \int_{d_n-a_n}^{d_n+a_n} \int_{-h}^{0} [\phi^S\left(b_n^+, y, z\right) - \phi^S\left(b_n^-, y, z\right)]u(z)dzdy \tag{2.19}$$

and

$$F_{m,n} = -i\omega\rho \int_{d_n-a_n}^{d_n+a_n} \int_{-h}^{0} [\phi^m\left(b_n^+, y, z\right) - \phi^m\left(b_n^-, y, z\right)]u(z)dzdy \tag{2.20}$$

for $n = 1, ..., N$.

We then further decompose $F_{m,n}$ into real and imaginary components

$$F_{m,n} = i\omega\mathcal{A}_{nm}(\omega) - \mathcal{B}_{nm}(\omega) \tag{2.21}$$

where the real quantities $A_{nm}(\omega)$ are each in phase with the acceleration of the nth flap due to the forced oscillatory motion of the mth, routinely being called the added inertia coefficients. Meanwhile, the real components $\mathcal{B}_{nm}(\omega)$ are the corresponding radiation damping coefficients and are in phase with the velocity of the nth flap due to the motion of the mth. Substituting back into (2.18) we have that the time-independent wave torque is given by

$$F_{w,n} = AF_{S,n} + \sum_{m=1}^{N} \left(i\omega\mathcal{A}_{nm} - \mathcal{B}_{nm}\right)\Omega_m. \tag{2.22}$$

Given the nature of the problem, in which we are considering an array of flap-type devices, it is natural to pursue a matrix formulation. To that end we let

$$\mathbf{A} = (\mathcal{A}_{nm}) \qquad \text{and} \qquad \mathbf{B} = (\mathcal{B}_{nm}) \tag{2.23}$$

denote the real, symmetric $N \times N$ added inertia and radiation damping matrices and

$$\mathbf{M} = \text{diag}\left(I_1, I_2, ..., I_N\right) \qquad \text{and} \qquad \mathbf{C} = \text{diag}\left(C_1, C_2, ..., C_N\right) \tag{2.24}$$

be diagonal matrices with elements comprised of the moments of inertia and restoring torques of each of the N flaps. Further, we define the following complex N-vectors

$$\mathbf{F}_S = A\left(F_{S,1}, F_{S,2}, ..., F_{S,N}\right)^T \qquad \text{and} \qquad \mathbf{\Omega} = \left(\Omega_1, \Omega_2, ..., \Omega_N\right)^T \tag{2.25}$$

which allow us to define the vector of wave forces as

$$\mathbf{F}_w = \mathbf{F}_S + \left(i\omega\mathbf{A} - \mathbf{B}\right)\mathbf{\Omega}. \tag{2.26}$$

Thus far we have not considered the mechanism for power take-off. For now, we decide that it should take a general form and be written as

$$\mathbf{F}_e = -\mathbf{\Lambda}\mathbf{\Omega} \tag{2.27}$$

so that the force due to power take-off on the nth flap is a linear combination of forces proportional to the angular velocities of all N flaps. This is governed by the controllable power take-off matrix $\mathbf{\Lambda}$ for which we wish to determine optimal values. Employing our matrix notation and expressions for the external mechanical and wave torques we may rewrite equation (2.16) as

$$\mathbf{F}_S = \left(\mathbf{B} - i\omega\left(\mathbf{A} + \mathbf{M} - \frac{1}{\omega^2}\mathbf{C}\right)\right)\mathbf{\Omega} + \mathbf{\Lambda}\mathbf{\Omega}. \tag{2.28}$$

The notation may be further streamlined by defining the following complex, symmetric matrix

$$\mathbf{Z} = \mathbf{B} - i\omega\left(\mathbf{A} + \mathbf{M} - \frac{1}{\omega^2}\mathbf{C}\right), \tag{2.29}$$

which gives the exciting force vector to be

$$\mathbf{F}_S = (\mathbf{Z} + \mathbf{\Lambda})\,\mathbf{\Omega}. \tag{2.30}$$

Using that the time averaged power is given by

$$W = \frac{1}{2}\Re e\left\{\mathbf{F}_w^\dagger \mathbf{\Omega}\right\} = \frac{1}{2}\Re e\left\{\mathbf{F}_S^\dagger \mathbf{\Omega}\right\} - \frac{1}{2}\mathbf{\Omega}^\dagger \mathbf{B}\mathbf{\Omega} \tag{2.31}$$

then after some manipulation it may be shown (see for example, Evans [6]) that

$$W = \frac{1}{8}\mathbf{F}_S^\dagger\left[\mathbf{B}^{-1} - \mathbf{E}^\dagger\mathbf{B}^{-1}\mathbf{E}\right]\mathbf{F}_S \qquad \text{where} \qquad \mathbf{E} = \left(\mathbf{Z}^\dagger - \mathbf{\Lambda}\right)\left(\mathbf{\Lambda} + \mathbf{Z}\right)^{-1}. \tag{2.32}$$

Here the dagger notation has been used for the adjoint (or conjugate transpose) of a matrix. By inspection of this form for the power we may easily see that the maximum is given by

$$W_{max} = \frac{1}{8}\mathbf{F}_S^\dagger \mathbf{B}^{-1}\mathbf{F}_S \tag{2.33}$$

which is achieved when the condition $\mathbf{\Lambda} = \mathbf{Z}^\dagger$ is satisfied. However, this requires $\mathbf{\Lambda}$ to be a dense, complex matrix which gives rise to fundamental issues in terms of the practical implementation. Firstly, due to the non-zero off-diagonal elements, the damping which is applied to the nth flap depends on the complex angular velocity of all N flaps. This requires them to be be linked and would be impractical in reality. Secondly, the complex values require a phase-lag between power and velocity. Thus the form given in (2.31) has limited practical use and it is arguably simpler to compute the power using (2.16) in (2.31) first to give

$$W = -\frac{1}{2}\Re e\left\{\mathbf{F}_e^\dagger \mathbf{\Omega}\right\} = \frac{1}{2}\Re e\left\{\mathbf{F}_S^\dagger\left(\mathbf{Z}^\dagger + \mathbf{\Lambda}\right)^{-1}\mathbf{\Lambda}\left(\mathbf{Z} + \mathbf{\Lambda}\right)^{-1}\mathbf{F}_S\right\} \tag{2.34}$$

in which the second equality results after using (2.27) and (2.30) and the assumption that $\mathbf{\Lambda}$ is real. In Appendix A we go on to consider particular practical forms for $\mathbf{\Lambda}$, in each case deriving equations determining optimal values. In general these are not closed form but implicit. However, for two identical, parallel devices we are able to establish analytic bounds for the optimal power take-off parameter $\mathbf{\Lambda}$.

At this point we focus on the calculation of the power. This requires the determination of certain hydrodynamic coefficients, namely the exciting force on a fixed flap, F_S, along with the added inertia and radiation damping matrices, $\mathbf{A}$ and $\mathbf{B}$. These are found through the solution of the hydrodynamic problems for ϕ^S and ϕ^m, $m = 1, ..., N$.

3. Specification of the Scattering and Radiation Problems

3.1. The Scattering Problem

The scattering problem deals with the diffraction of the incident wave when the flaps are held fixed vertically. The problems for both a single fixed barrier and a periodic array have previously been considered by many authors (for example Morse and Rubenstein [13] and Carr and Stelzriede [3] in the first case and Porter and Evans [14] and Williams and Crull [23] in the second).

First, we extract the depth dependence since the flaps extend uniformly throughout the entire depth, remaining in a fixed vertical position. We do this by writing the velocity potential associated with the scattering problem as

$$\phi^S(x,y,z) = \psi^S(x,y)\,\psi_0(z). \tag{3.1}$$

Thus (2.9) reduces to the modified Helmholtz equation,

$$\left(\frac{\partial^2}{\partial x^2} + \frac{\partial^2}{\partial y^2} + k^2\right)\psi^S = 0, \tag{3.2}$$

in the plane of the free surface. Both the combined linear free surface condition (2.10) and the bottom condition (2.11) are automatically satisfied by (3.1), leaving the condition on the flap itself (2.12) which becomes

$$\psi_x^S\left(b_n^{\pm}, y\right) = 0 \qquad \text{for } y \in \left[d_n - a_n, d_n + a_n\right],\ n = 1, ..., N. \tag{3.3}$$

It can be seen immediately from (2.14) that the incident wave may be represented by

$$\psi^I = e^{-ik(x\cos\beta - y\sin\beta)}. \tag{3.4}$$

Then the exciting wave torque about the pivot of the nth flap is given, from (2.19), by

$$F_{S,n} = -i\omega\rho\int_{a_n-d_n}^{a_n+d_n}\int_{-h}^{0}\left[\psi^D\left(b_n^+, y\right) - \psi^D\left(b_n^-, y\right)\right]\psi_0(z)\,u(z)\,dzdy \quad \text{for } n = 1, ..., N, \tag{3.5}$$

where $\psi^D \equiv \psi^S - \psi^I$ represents the diffracted potential and is characterised by outgoing waves at infinity. It is helpful to decompose $u(z)$ in terms of the complete set of normalised depth eigenfunctions

$$\psi_j(z) = N_j^{-1/2}\cos k_j(z+h), \qquad N_j = \frac{1}{2}\left(1 + \frac{\sin 2k_k h}{2k_j h}\right) \tag{3.6}$$

where k_j for $j = 1, 2, ...$ are the positive roots of $\omega^2 = -gk_j\tan k_j h$. This is consistent with the definition given for $\psi_0(z)$ in (2.15) if we let $k_0 = -ik$. The normalised depth eigenfunctions $\psi_j(z)$, including $j = 0$, satisfy the orthogonality relation

$$\frac{1}{h}\int_{-h}^{0}\psi_i(z)\,\psi_j(z)\,dz = \delta_{ij}. \tag{3.7}$$

We can then write

$$u(z) = \sum_{j=0}^{\infty} U_j\psi_j(z), \tag{3.8}$$

where, using the definition of $u(z)$ from (2.4), we have

$$U_j = \frac{1}{h}\int_{-h}^{0}u(z)\psi_i(z)dz = \frac{N_j^{-1/2}}{k_j^2 h}\left(k_j c\sin k_j h + \cos k_j h - \cos k_j(h-c)\right). \tag{3.9}$$

Finally, substituting $u(z)$ as expressed in (3.8) into the integral (2.20) and using the orthogonality relation (3.7), the z integral evaluates to hU_0. This results in the exciting torque (2.20) on each of the N flaps reducing to

$$F_{S,n} = -i\omega\rho U_0 h\int_{d_n-a_n}^{d_n+a_n}\left[\psi^D\left(b_n^+, y\right) - \psi^D\left(b_n^-, y\right)\right]dy \qquad \text{for } n = 1, ..., N. \tag{3.10}$$

3.2. The Radiation Problem

The remaining components in the decomposition of the velocity potential deal with the waves radiated when each of the flaps in turn undergoes a prescribed oscillatory motion whilst all others remain fixed. The linearised kinematic condition on the flap extends throughout the entire depth and depends only on z. Using the decomposition of $u(z)$ this gives

$$\phi_x^m\left(b_n^{\pm}, y, z\right) = \delta_{mn}\sum_{j=0}^{\infty} U_j\psi_j\left(z\right) \quad \text{for}\, y \in \left(d_n - a_n, d_n + a_n\right),\, z \in (-h, 0) \,\text{and}\, n, m = 1, ..., N. \tag{3.11}$$

On account of (3.11), we may express the potential everywhere as a superposition of modes associated with the same set of depth modes

$$\phi^m\left(x, y, z\right) = \sum_{j=0}^{\infty} U_j\phi_j^m\left(x, y\right)\psi_j\left(z\right) \qquad \text{for } m = 1, ..., N. \tag{3.12}$$

Returning to our governing equations we now have, using the definition of $\psi_j(z)$ given in (3.6) and independence of the solutions,

$$\left(\frac{\partial^2}{\partial x^2} + \frac{\partial^2}{\partial y^2} - k_j^2\right)\phi_j^m = 0 \qquad \text{for } j = 0, 1, 2, ... \text{ and } m = 1, ..., N \tag{3.13}$$

in the plane of the free surface. The linearised kinematic condition, using (3.11) and (3.12), becomes

$$\frac{\partial\phi_j^m}{\partial x}\left(b_n^{\pm}, y; \beta\right) = \delta_{mn} \qquad \text{for } y \in \left(d_n - a_n, d_n + a_n\right),\; z \in (-h, 0) \text{ and } m, n = 1, ..., N. \tag{3.14}$$

Finally, using (2.4), (3.8) and (3.12), the wave torque about the pivot on the nth flap due to the prescribed oscillatory motion of the mth flap (2.20) becomes

$$F_{m,n} = -i\omega\rho h\sum_{j=0}^{\infty} U_j^2\int_{d_n-a_n}^{d_n+a_n}\left[\phi_j^m\left(b_n^+, y\right) - \phi_j^m\left(b_n^-, y\right)\right]dy \qquad \text{for } n, m = 1, ..., N. \tag{3.15}$$

4. Derivation of Integral Equations

4.1. The Scattering Problem

Methods based on Green's functions applied to the solution to the wave equation are well known and versatile, particularly when applied to scattering of waves by geometries with complex shapes. Here we will take advantage of the geometry being considered, in which the N-flaps are all thin and arranged parallel to each other, to apply a more direct solution using Fourier transforms . We define the Fourier transform of $\psi^D(x, y)$ by

$$\overline{\psi}^D(x, l) = \int_{-\infty}^{\infty}\psi^D(x, y)e^{-ily}dy. \tag{4.1}$$

Then, taking Fourier transforms with respect to y of the governing Helmholtz equation (3.2) gives

$$\left(\frac{d^2}{dx^2} + \left(k^2 - l^2\right)\right)\overline{\psi}^D = 0. \tag{4.2}$$

We proceed by assuming a general arrangement of flaps in which each flap is displaced laterally from neighbouring flaps. That is, $b_1 < b_2 < ... < b_N$ and the domain is divided into $N+1$ sections denoted by χ_ν, $\nu = 1, ..., N+1$ as shown in figure 2. These are separated by vertical planes in line with each of the barriers at $x = b_n$, $n = 1, ..., N$. It turns out that the special case in which one or more flaps occupy the same plane can be recovered from the final system simply by setting

$b_n = b_m$ for $m \neq n$. Solving the Fourier transformed Helmholtz equation (4.2) in each of the domains gives

$$\overline{\psi}^D(x,l) = \begin{cases} A_1(l)e^{\lambda(x-b_1)} & \text{for } -\infty < x < b_1 \\ A_\nu(l)e^{\lambda x} + B_\nu(l)e^{-\lambda x} & \text{for } b_{\nu-1} < x < b_\nu, \nu = 2, ..., N \\ B_{N+1}(l)e^{-\lambda(x-b_N)} & \text{for } b_N < x < \infty \end{cases} \tag{4.3}$$

where $B_1 = A_{N+1} = 0$ so that the solution remains bounded as $x \to \pm\infty$. Also,

$$\lambda(l,k) = \sqrt{l^2 - k^2} = -i\sqrt{k^2 - l^2}, \qquad \text{when } |l| < k, \tag{4.4}$$

where the choice of branch ensures the radiation condition is satisfied. By continuity of $\overline{\psi}^D_x$ across $x = b_n$ for $n = 1, ..., N$ we may derive a set of N linear equations for the unknowns $A_\nu(l)$ and $B_\nu(l)$, $\nu = 1, ..., N+1$,

$$A_1(l) = A_2(l)e^{\lambda b_1} - B_2(l)e^{-\lambda b_1} \qquad \text{when } \nu = 1, \tag{4.5}$$

$$A_\nu(l)e^{\lambda b_\nu} - B_\nu(l)e^{-\lambda b_\nu} = A_{\nu+1}(l)e^{\lambda b_\nu} - B_{\nu+1}(l)e^{-\lambda b_\nu} \qquad \text{for } \nu = 2, ..., N-1, \text{ and} \tag{4.6}$$

$$A_N(l)e^{\lambda b_N} - B_N(l)e^{-\lambda b_N} = -B_{N+1}(l) \qquad \text{when } \nu = N. \tag{4.7}$$

Further, defining N functions related to the pressure differences across each of the flaps,

$$P_n(y) = \psi^D\left(b_n^+, y\right) - \psi^D\left(b_n^-, y\right) \qquad \text{for } n = 1, ..., N, \tag{4.8}$$

taking Fourier transforms and using our Fourier transformed solutions (4.3), we may produce an additional N linear equations for our unknowns

$$\overline{P}_n(l) = \begin{cases} A_2(l)e^{\lambda b_1} + B_2(l)e^{-\lambda b_1} - A_1(l) & \text{for } n = 1, \\ A_{n+1}(l)e^{\lambda b_n} + B_{n+1}(l)e^{-\lambda b_n} - A_n(l)e^{\lambda b_n} - B_n(l)e^{-\lambda b_n} & \text{for } n = 2, ..., N-1, \\ B_{N+1}(l) - A_N(l)e^{\lambda b_N} - B_N(l)e^{-\lambda b_N} & \text{for } n = N, \end{cases} \tag{4.9}$$

where the Fourier transformed pressure difference is defined by

$$\overline{P}_\nu(l) = \int_{d_\nu - a_\nu}^{d_\nu + a_v} P_\nu(y)e^{-ily}\, dy. \tag{4.10}$$

This complete set of $2N$ linear equations may be solved for our unknowns surprisingly simply to give

$$\overline{\psi}^D(x,l) = \begin{cases} -\frac{1}{2}\sum_{\nu=1}^{N} e^{-\lambda(b_\nu - x)}\overline{P}_\nu(l) & \text{for } -\infty < x < b_1 \\ \frac{1}{2}\sum_{\nu=1}^{n-1} e^{\lambda(b_\nu - x)}\overline{P}_\nu(l) - \frac{1}{2}\sum_{\nu=n}^{N} e^{-\lambda(b_\nu - x)}\overline{P}_\nu(l) & \text{for } b_{n-1} < x < b_n, n = 2, ..., N \\ \frac{1}{2}\sum_{\nu=1}^{N} e^{\lambda(b_\nu - x)}\overline{P}_\nu(l) & \text{for } b_N < x < \infty. \end{cases} \tag{4.11}$$

At this point we invoke the inverse Fourier transform to give an integral representation for $\psi^D(x,y)$ applicable throughout the $N+1$ sections of the domain, namely

$$\psi^D(x,y) = \frac{1}{4\pi}\sum_{\nu=1}^{N} sgn(x - b_\nu)\int_{-\infty}^{\infty} e^{-\lambda|x-b_\nu|}e^{ily}\overline{P}_\nu(l)dl \tag{4.12}$$

$$= \frac{1}{4\pi}\sum_{\nu=1}^{N} sgn(x - b_\nu)\int_{-\infty}^{\infty} e^{-\lambda|x-b_\nu|}e^{ily}\int_{d_\nu - a_\nu}^{d_\nu + a_\nu} P_\nu(y')e^{-ily'}dy'dl. \tag{4.13}$$

We now apply the following condition

$$\frac{\partial\psi^D}{\partial x}(b_n^\pm, y) = -\frac{\partial\psi^I}{\partial x}(b_n^\pm, y) \qquad \text{for } n = 1, ..., N \tag{4.14}$$

which ensures zero velocity on each of the stationary flaps. This results in the following N coupled integral equations for $P_\nu(y)$,

$$-\frac{\partial \psi^I}{\partial x}(b_n, y) = -\frac{1}{4\pi}\sum_{\nu=1}^{N}\int_{-\infty}^{\infty}\lambda(l,k)\,e^{-\lambda|b_n-b_\nu|}e^{ily}\int_{d_\nu-a_\nu}^{d_\nu+a_\nu}P_\nu(y')\,e^{-ily'}dy'dl, \tag{4.15}$$

for $n = 1, ..., N$. Bearing in mind the known end-point behaviour of the pressure difference across each of the flaps, $P_\nu(y) \sim \left(a_\nu^2 - (y-d_\nu)^2\right)^{1/2}$ as $y \to d_\nu \pm a_\nu$, it may be shown that the inner integral behaves like $O\left(|l|^{-3/2}\right)$ for large $|l|$. This behaviour of the inner integral in turn ensures the convergence of the outer integral. It is important to note that the order of integration in (4.15) may not be interchanged as this leads to divergent integrals. We may not solve this set of integral equations analytically, instead we now consider a numerical solution method, introducing expansions for the unknowns

$$P_\nu(y) \approx \sum_{p=0}^{2P+1}\alpha_p^{(\nu)}w_p\left(\frac{y-d_\nu}{a_\nu}\right) \qquad \text{for } d_\nu - a_\nu < y < d_\nu + a_\nu \qquad \text{and} \qquad \nu = 1, ..., N, \tag{4.16}$$

where

$$w_p(t) = \frac{e^{i\pi p/2}}{(p+1)}\sqrt{1-t^2}U_p(t) \qquad \text{and} \qquad U_p(\cos\theta) = \frac{\sin(p+1)\theta}{\sin\theta}$$

are Chebychev polynomials of the second kind. Here, the known end-point behaviour of $P_\nu(y)$ has been incorporated into the orthogonal basis functions $w_p(t)$ along with numerical scaling factors which anticipate later algebraic simplification. In order to determine the new set of unknowns $\alpha_p^{(\nu)}$ we first substitute (4.16) into (4.15) to give

$$\frac{\partial \psi^I}{\partial x}(b_n, y) = \frac{1}{4\pi}\sum_{p=0}^{2P+1}\sum_{\nu=1}^{N}\alpha_p^{(\nu)}\int_{-\infty}^{\infty}\lambda(l,k)\,e^{-\lambda|b_n-b_\nu|}e^{ily}\int_{d_\nu-a_\nu}^{d_\nu+a_\nu}w_p\left(\frac{y'-d_\nu}{a_\nu}\right)e^{-ily'}dy'dl, \tag{4.17}$$

for $n = 1, ..., N$. Then, as is typical of the Galerkin method, we multiply the nth equation through by $(-1/\pi)\,w_q^*\left((y-d_n)/a_n\right)$ and integrate over the corresponding domain $y \in (d_n - a_n, d_n + a_n)$ to give the following system of equations for the coefficients $\alpha_p^{(\nu)}$:

$$\sum_{p=0}^{2P+1}\sum_{\nu=1}^{N}\alpha_p^{(\nu)}K_{qp}^{(n\nu)} \simeq D_q^{(n)} \tag{4.18}$$

for $q = 0, 1, ..., 2P+1$ and $n = 1, ..., N$ where

$$K_{qp}^{(n\nu)} = \frac{1}{4\pi^2}\int_{-\infty}^{\infty}\lambda(l,k)e^{-\lambda|b_n-b_\nu|}\int_{d_n-a_n}^{d_n+a_n}w_q^*\left(\frac{y-d_n}{a_n}\right)e^{ily}dy\int_{d_\nu-a_\nu}^{d_\nu+a_\nu}w_p\left(\frac{y'-d_\nu}{a_\nu}\right)e^{-ily'}dy'dl \tag{4.19}$$

and

$$D_q^{(n)} = -\frac{1}{\pi}ik\cos\beta e^{-ikb_n\cos\beta}\int_{d_n-a_n}^{d_n+a_n}e^{iky\sin\beta}w_q^*\left(\frac{y-d_n}{a_n}\right)dy. \tag{4.20}$$

Using Gradshteyn and Ryzhik [10§3.715 (13), (18)], for example, along with properties of the Bessel functions J_q, we may derive the following integral identity

$$\int_{-a}^{a}e^{ilx}\left(a^2-\xi^2\right)^{1/2}U_p\left(\frac{\xi}{a}\right)d\xi = \begin{cases}\dfrac{e^{in\pi/2}(p+1)\pi a^2}{al}J_{p+1}(al) & \text{if } l \neq 0\\ \frac{1}{2}a^2\pi\delta_{p0} & \text{if } l = 0.\end{cases} \tag{4.21}$$

This can then be used to evaluate the integrals in (4.19) and (4.20) and ultimately we arrive at the results

$$K_{qp}^{(n\nu)} = \frac{1}{4}\int_{-\infty}^{\infty} \frac{\lambda(l,k)}{l^2} e^{-\lambda|b_n - b_\nu|} e^{il(d_n - d_\nu)} J_{p+1}(a_\nu l)\, J_{q+1}(a_n l)\, dl \tag{4.22}$$

and

$$D_q^{(n)} = \begin{cases} -\dfrac{ie^{ik(d_n \sin\beta - b_n \cos\beta)} J_{q+1}(ka_n \sin\beta)}{\tan\beta} & \text{if } \beta \neq 0 \\ \dfrac{1}{2} ika_n e^{-ikb_n} \delta_{q0} & \text{if } \beta = 0. \end{cases} \tag{4.23}$$

It may be seen that the integrals giving $K_{qp}^{(n\nu)}$ are exponentially convergent in all cases except when $\nu = n$ (assuming for the moment $b_n \neq b_\nu$ for $n \neq \nu$). In this case we note that $K_{pq}^{(nn)} = 0$ if $p+q$ is odd and so we may reduce our consideration to elements for which $p+q$ is even. Then we use an integral result involving products of Bessel functions [10§6.5382(2)] to write

$$K_{2q+\mu,2p+\mu}^{(nn)} = \frac{\delta_{pq}}{8q+4+4\mu} + \tilde{K}_{2q+\mu,2p+\mu}^{(nn)} \tag{4.24}$$

where

$$\tilde{K}_{2q+\mu,2p+\mu}^{(nn)} = \frac{1}{2}\int_0^{\infty} \left(\frac{\lambda(l,k)}{l^2} - \frac{1}{l} \right) J_{2p+1+\mu}(a_n l) J_{2q+1+\mu}(a_n l) dl \tag{4.25}$$

for $\mu = 0, 1$ and $p, q = 0, 1, ...$ This ensures more rapid convergence, with the integrand decaying like $O\left((ka_n)^2 / l^4\right)$, and finally results in (4.18) reducing to the following coupled pair of systems

$$\frac{\alpha_{2q}^{(n)}}{8q+4} + \sum_{p=0}^{P} \left\{ \alpha_{2p}^{(n)} \tilde{K}_{2q,2p}^{(nn)} + \sum_{\substack{\nu=1 \\ \nu\neq n}}^{N} \left[K_{2q,2p}^{(n\nu)} \alpha_{2p}^{(\nu)} + K_{2q,2p+1}^{(n\nu)} \alpha_{2p+1}^{(\nu)} \right] \right\} = D_{2q}^{(n)} \tag{4.26}$$

and

$$\frac{\alpha_{2q+1}^{(n)}}{8q+8} + \sum_{p=0}^{P} \left\{ \alpha_{2p+1}^{(n)} \tilde{K}_{2q+1,2p+1}^{(nn)} + \sum_{\substack{\nu=1 \\ \nu\neq n}}^{N} \left[K_{2q+1,2p+1}^{(n\nu)} \alpha_{2p+1}^{(\nu)} + K_{2q+1,2p}^{(n\nu)} \alpha_{2p}^{(\nu)} \right] \right\} = D_{2q+1}^{(n)} \tag{4.27}$$

for $q = 0, ..., P$. This coupled pair of systems determining for our unknowns $\alpha_p^{(n)}$, $p = 0, ..., 2P+1$, $n = 1, ..., N$ are now second-kind in structure. Finally, substituting (4.16) into (3.10), the exciting torque induced on the nth flap may now be expressed in terms of the Galerkin expansion coefficients as

$$F_{S,n} = -\frac{1}{2} i\omega\rho U_0 h \alpha_0^{(n)} a_n \pi \qquad \text{for } n = 1, ..., N. \tag{4.28}$$

4.2. The Radiation Problem

The solution method for the remaining wave torques, associated with the radiation problem, follows similarly to the scattering problem. We follow the method used previously to derive the integral equations for $\phi_m^j(b_n^+, y)$ in $d_n - a_n < y < d_n + a_n$ as

$$\delta_{mn} = \frac{\partial \phi_j^m}{\partial x}(b_n^+, y) = -\frac{1}{4\pi} \sum_{\nu=1}^{N} \int_{-\infty}^{\infty} \gamma(l, k_j)\, e^{-\gamma|b_n - b_\nu|} e^{ily} \int_{d_\nu - a_\nu}^{d_\nu + a_\nu} P_{m\nu}^j(y') e^{-ily'} dy' dl \tag{4.29}$$

for $n, m = 1, ..., N$ and $j = 0, 1, ...$. The significant differences from the scattering problem are the replacement of $\lambda(l,k)$ with $\gamma(l,k_j) \equiv \sqrt{l^2 + k_j^2}$ and the revised forcing term which ensures zero

velocity on each of the stationary flaps whilst also satisfying the linearised kinematic condition on the mth flap, which is undergoing prescribed oscillatory motion.

We have also defined a new set of functions each related to the pressure difference across the nth flap due to the oscillatory motion of the mth flap when all others are held fixed,

$$P^j_{mn}(y) = \phi^m_j(b^+_n, y) - \phi^m_j(b^-_n, y) \qquad \text{for} \qquad n, m = 1, ..., N \qquad \text{and} \quad i = 0, 1, 2, \dots . \tag{4.30}$$

The potential may then be found to be

$$\phi^m_j(x, y) = \frac{1}{4\pi} \sum_{\nu=1}^{N} sgn(x - b_\nu) \int_{-\infty}^{\infty} e^{-\gamma|x-b_\nu|} e^{ily} \int_{d_\nu - a_\nu}^{d_\nu + a_\nu} P^j_{m\nu}(y') e^{-ily'} dy' dl. \tag{4.31}$$

We again assume a Galerkin expansion for our unknown functions, given in (4.30), related to the pressure difference across the νth flap when the mth flap is free to oscillate. This is expressed in terms of the same set of orthogonal basis functions, w_p, defined earlier in (4.16), but with a new set of unknown coefficients. At this point for ease of notation we drop the j superscript and henceforth will assume we are considering the jth mode. We write

$$P_{m\nu}(y) \simeq \sum_{p=0}^{2P+1} \alpha^{(m\nu)}_p w_p \left(\frac{y - d_\nu}{a_\nu} \right) \qquad \text{for } d_\nu - a_\nu < y < d_\nu + a_\nu,\ \nu = 1, 2, ..., N. \tag{4.32}$$

Following the same approximation methods as previously for the scattering problem we find the following system of equations for the coefficients $\alpha^{(m\nu)}_p$:

$$\sum_{p=0}^{2P+1} \sum_{\nu=1}^{N} \alpha^{(m\nu)}_p L^{(n\nu)}_{qp} \simeq E^{(nm)}_q. \tag{4.33}$$

Where, analogously to the scattering problem we have defined

$$L^{(n\nu)}_{qp} = \frac{1}{2} \int_{-\infty}^{\infty} \frac{\gamma(l, k_j)}{l^2} e^{-\gamma|b_n - b_\nu|} e^{il(d_n - d_\nu)} J_{p+1}(a_\nu l) J_{q+1}(a_n l) dl \tag{4.34}$$

and

$$E^{(nm)}_q = \delta_{mn} \delta_{q0} a_n \tag{4.35}$$

so that we may write our integral equations more compactly.

As for the scattering problem we find that the integrals are again exponentially convergent in all cases except where $\nu = n$ (again making the assumption for the moment that $b_n \neq b_\nu$ for $n \neq \nu$) and that $L^{(nn)}_{qp} = 0$ if $p + q$ is odd. The integral result from Gradshteyn and Ryzhik [10§6.5382(2)] is employed as before, for the non-zero elements, to write

$$L^{(nn)}_{2q+\mu, 2p+\mu} = \frac{\delta_{pq}}{8q + 4 + 4\mu} + \tilde{L}^{(nn)}_{2q+\mu, 2p+\mu} \tag{4.36}$$

where

$$\tilde{L}^{(nn)}_{2q+\mu, 2p+\mu} = \frac{1}{2} \int_0^{\infty} \left(\frac{\gamma(l, k_j)}{l^2} - \frac{1}{l} \right) J_{2p+1+\mu}(a_n l) J_{2q+1+\mu}(a_n l) dl \tag{4.37}$$

for $\mu = 0, 1$ and $p, q, = 0, 1, 2, \dots$. Which results in the following coupled pair of systems

$$\frac{\alpha^{(nm)}_{2q}}{4q + 2} + \frac{1}{2} \sum_{p=0}^{P} \left\{ \alpha^{(nm)}_{2p} \tilde{L}^{(nn)}_{2q, 2p} + \sum_{\substack{\nu=1 \\ \nu \neq n}}^{N} \left[L^{(n\nu)}_{2q, 2p} \alpha^{(m\nu)}_{2p} + L^{(n\nu)}_{2q, 2p+1} \alpha^{(m\nu)}_{2p+1} \right] \right\} = E^{(nm)}_{2q} \tag{4.38}$$

and

$$\frac{\alpha_{2q+1}^{(nm)}}{4q+2}+\frac{1}{2}\sum_{p=0}^{P}\left\{\alpha_{2p+1}^{(nm)}\tilde{L}_{2q+1,2p+1}^{(nn)}+\sum_{\substack{\nu=1\\ \nu\neq n}}^{N}\left[L_{2q+1,2p+1}^{(n\nu)}\alpha_{2p+1}^{(m\nu)}+L_{2q+1,2p}^{(n\nu)}\alpha_{2p}^{(m\nu)}\right]\right\}=E_{2q+1}^{(nm)} \quad (4.39)$$

for $q=0,...,P$, $m=1,...,N$ where, for fixed j, the integrand in (4.37) decays like $O((k_j a_n)^2/l^4)$. Here, $k_j\sim j\pi/h$ and so the integration range required is increased for larger values of j and a_n/h.

Finally, reintroducing the j superscript and identifying $\alpha_0^{(mn)j}\equiv\alpha_0^{(mn)}$ when applied to the jth mode, from (2.20) the wave torques are given by

$$F_{mn}=-i\omega\rho h a_n\pi\sum_{j=0}^{\infty}U_j^2\alpha_0^{(mn)j}. \quad (4.40)$$

5. Numerical Calculations

5.1. Angle of Excursion

The formulation is based on a linearised theory of water waves and there has been an *a priori* assumption that excursions of the flap from the vertical are small in order that the results retain validity. We must therefore be careful to ensure in the results presented that this assumption is justified. Here we consider the size of the response of nth device as a function of frequency and incident wave amplitude. We recall from (2.30) that

$$\boldsymbol{\Omega}=\left(\mathbf{Z}+\boldsymbol{\Lambda}\right)^{-1}\mathbf{F}_S \quad (5.1)$$

and so, since from (2.7) the maximum angle of excursion of the nth flap for a particular incident wave frequency is given by $|\Theta_n|=|\Omega_n/\omega|$, we have

$$\left|\frac{\Theta_n}{H}\right|=\frac{|\Omega_n|}{H\omega}=\frac{\left|\left(\left(\mathbf{Z}+\boldsymbol{\Lambda}\right)^{-1}\mathbf{F}_S\right)_n\right|}{H\omega}, \quad (5.2)$$

the (dimensional) measure of the maximum displaced angle of the flap per unit height of incident wave.

5.2. Irregular Waves

Throughout the results presented later we consider the optimal device performance when subject to irregular waves. To do this we need to introduce a wave energy spectrum $S(T)$ which is used to represent a more realistic sea state. We choose the Bretschneider Spectrum (Bretschneider [2]),

$$S_{BS}(T)=\frac{5}{6}H_{\frac{1}{3}}^2\frac{T^5}{T_p^4}e^{-\frac{5}{4}(T/T_p)^4}, \quad (5.3)$$

which was designed to model seas over long fetches that are not necessarily fully developed. This is appropriate to the wave energy sites off the coast of the UK where waves are incident from the Atlantic ocean. Here $H_{\frac{1}{3}}$ denotes the significant wave height, that is the mean height of the highest one third of waves, and T_p is the peak wave period in the spectrum. However, since the Bretschneider Spectrum is designed to model deep water, an additional depth dependent factor is introduced. This is of the form suggested by Bouws et al. [1] for the JONSWAP (Joint North Sea Wave Project) spectrum and produces a self similar spectrum which favours shorter wavelengths in shallower water. Thus we employ the following adapted spectrum,

$$S(T)=\phi_K\left(f_H\right)S_{BS}(T), \quad (5.4)$$

where

$$\phi_K(f) = \frac{\left[(k(f,H))^{-3}\,\frac{\partial k(f,H)}{\partial \omega}\right]}{\left[(k(f,\infty))\,\frac{\partial k(f,\infty)}{\partial \omega}\right]} \tag{5.5}$$

and

$$f_H = 2\pi\omega\sqrt{\frac{H}{g}}. \tag{5.6}$$

Finally, the directional spread of incident waves in the nearshore environment is incorporated using a normalised cosine curve spanning $\pm\pi/6$ radians ($\pm 30°$) to model the predominantly normally incident wave fronts,

$$E(T,\beta) = S(T)D(\beta) \qquad \text{where} \qquad D(\beta) = \begin{cases} \frac{3}{\pi}(\cos(6\beta)+1) & \text{if } -\frac{\pi}{6} < \beta < \frac{\pi}{6} \\ 0 & \text{otherwise.} \end{cases} \tag{5.7}$$

The mean incident wave power per unit crest length for this spectrum is given by

$$\overline{W}_{inc} = 2\pi\rho g \int_{-\frac{\pi}{6}}^{\frac{\pi}{6}} \int_0^\infty c_g(T) E(T,\beta) T^{-2}\, dT\, d\beta \tag{5.8}$$

whilst the average power absorbed by an array of N wave surge converters is

$$\overline{W} = 2\pi\rho g \int_{-\frac{\pi}{6}}^{\frac{\pi}{6}} \int_0^\infty c_g(T) E(T,\beta) l(T,\beta) T^{-2}\, dT\, d\beta. \tag{5.9}$$

Here $l(T,\beta)$ is the single-frequency capture width of the array, expressed as a function of both wave period and angle of incidence, and $c_g(T)$ denotes the finite depth group velocity, expressed as function of the wave period. Combining these expressions we can define a mean capture factor which is non-dimensionalised by the total length of the devices in the array

$$\bar{l} = \frac{\overline{W}}{\overline{W}_{inc} \sum_{n=1}^{N} 2a_n}. \tag{5.10}$$

We will aim to maximise this quantity subject to some physical constraints and assumptions about the sea state.

We choose a model sea state determined by the parameters $H_{\frac{1}{3}} = 2.83m$ and $T_p = 9s$ as suggested by Falnes [8] consistent with an annual average power of approximately

$$W = \frac{\rho g^2 H_{\frac{1}{3}}^2 T_p}{64\pi} \simeq 30kW/m. \tag{5.11}$$

5.3. The physical parameters of the device

Having treated the flaps as infinitely thin for the solution of the hydrodynamic problem, we now give each device a width $2w_n$ to enable us to specify their physical properties such as mass, moment of inertia and buoyancy torque. All flaps are assumed to have the same mean density ρ_s and to extend from their pivots, located at identical depths $z = -c$, to the mean free surface level. The nth device has mass $M_{s,n} = 4\rho_s w_n c a_n$ with the moment of inertia about its pivot given by $I_n = \frac{1}{3}M_{s,n}(c^2 + w_n^2)$. The mass of water displaced by the flap is given by $M_{w,n} = 4\rho w_n c a_n$ where the fluid has density ρ and the constant of proportionality in the buoyancy torque of the nth device is then $C_n = \frac{1}{2}M_{w,n}(1-s)gc$. Here $s = \rho_s/\rho = M_{s,n}/M_{w,n}$ denotes the specific gravity of the flap.

We define the following matrices of dimensionless quantities

$$\hat{\mathcal{A}} = \frac{3}{c^2}\mathbf{M}_w^{-1}\mathcal{A}, \qquad \hat{\mathcal{B}} = \frac{3}{c^2\omega}\mathbf{M}_w^{-1}\mathcal{B}, \qquad \text{and} \qquad \hat{\mathbf{\Lambda}} = \frac{3}{c^2\omega}\mathbf{M}_w^{-1}\mathbf{\Lambda} \tag{5.12}$$

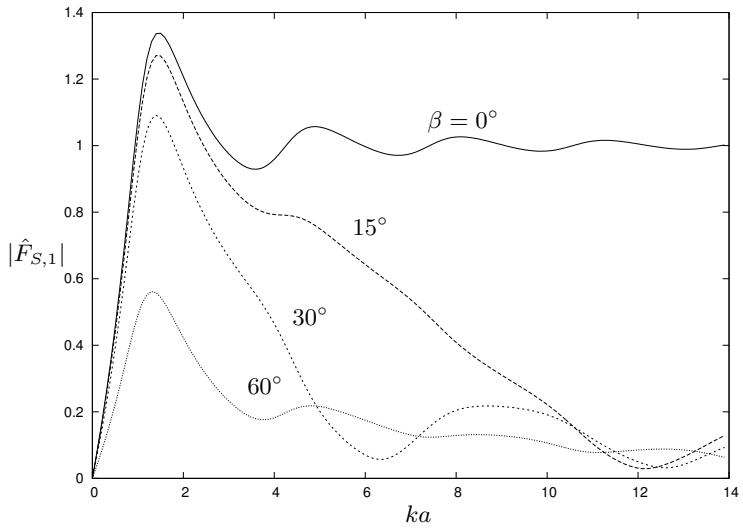

Figure 3: Modulus of dimensionless exciting torque on a fixed barrier against ka for different angles of incidence, $\beta = 0°, 15°, 30°, 60°$, as indicated.

where

$$\mathbf{M}_w = diag\,(M_{w,n}) \tag{5.13}$$

is the matrix with diagonal elements given by the mass of water displaced by each of the N flaps. Thus, $\mathbf{Z}$ becomes

$$\hat{\mathbf{Z}} = \frac{3}{c^2\omega}\mathbf{M}_w^{-1}\mathbf{Z} \tag{5.14}$$

and

$$\hat{F}_{S,n} = F_{S,n}/\left(4i\rho\omega U_0 h a_n\right) \qquad \text{for } n = 1, ..., N. \tag{5.15}$$

This non-dimensionalises the torque on the nth flap by the torque induced by normally incident waves on a section of the same length $2a_n$ of an infinitely long flap.

In addition to these non-dimensionalisations we decide that the power take-off should take the form $\mathbf{\Lambda} = \lambda\mathbf{I}$ for the purpose of the results presented. The assumption we are making in this choice is that all devices will have identical power take-off. This is representative of a practical power take-off system and simplifies the mathematics by reducing the number of free parameters and focusing our attention. The power may then be calculated using the form derived in the Appendix.

6. Results

6.1. A Single Device

The main focus of this paper is the optimisation of arrays of flap-type oscillating wave surge converters. However, it is useful to first consider a single device. This allows us to appraise the accuracy of the solution method, to consider the factors which play a role in the success of flap-type converters and to establish optimal device parameters which are then used in determining optimal array configurations and spacings. We therefore fix $N = 1$ for this section and, for the sake of simplicity, centre the flap at the origin so that $(b_1, d_1) = (0, 0)$.

According to the non-dimensionalisation given in (5.15) the dimensionless exciting torque, (4.28), is given by $\hat{F}_{S,1} = -\frac{1}{8}\pi\alpha_0$. This is independent of the geometrical parameters of the flap, instead depending only on ka and β. In figure 3 $|\hat{F}_{S,1}|$ is plotted as a function of ka for a range

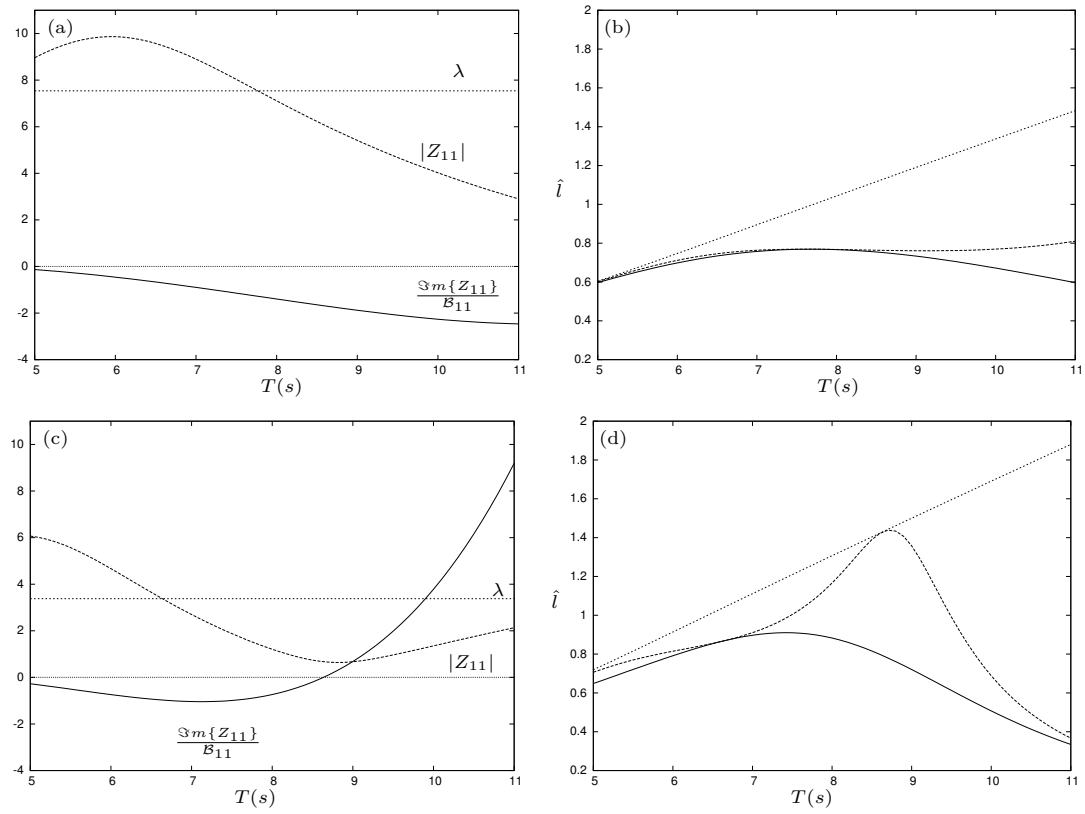

Figure 4: Variation of: (a) $|Z_{11}|$ and $\Im m\{Z_{11}\}/\mathcal{B}_{11}$, and (b) capture factors $\hat{l}_{max}$, $\hat{l}_{opt}$ and $\hat{l}$ with period T in seconds for optimal flap parameters, shown in table 1. The first two figures show results for device configuration 1 and the second two those for device configuration 2.

of incident wave angles, $\beta = 0°, 15°, 30°$ and $60°$, demonstrating agreement with known limiting behaviours. Firstly, considering normal incidence ($\beta = 0°$) we see that as ka increases, and the device becomes long compared to the incident wavelength, the torque tends to the two-dimensional limit i.e. the torque for a section of equivalent length from an infinitely-long flap. On the other hand as $ka \to 0$, and the device becomes small compared with the incident wavelength, then the torque tends to zero for all incident wave directions as expected. Considering the effect of the angle of incidence we may further note that as $\beta \to 90°$ and the incident waves become increasingly oblique the torque again tends to zero.

The numerical method used depends on various numerical truncation parameters. The infinite integrals defining matrix entries have been computed using 10-point Gauss quadrature on a truncated integration range and with a discretisation scheme which resolves the 2π-oscillation period of Bessel functions. Numerical experimentation suggests that as few as $n = 6$ evanescent modes in the radiation problem and $P = 6$ modes in the Galerkin approximation are sufficient to achieve results which are accurate enough for graphical purposes in all cases presented. Accurate results are very quick to compute. Results have been computed independently using a collocation method applied to a hypersingular integral equation formulation to verify their accuracy (personal communication, Dr Nicholas Biggs).

Having established confidence in the accuracy of the results we now turn our attention to the optimal performance of a single device. We first consider the single-frequency capture factor of the flap as a measure of its performance. This is given by

$$\hat{l} = \hat{l}_{max} \frac{2\mathcal{B}_{11}}{\mathcal{B}_{11} + |Z_{11}|} \left(1 - \frac{(\lambda - |Z_{11}|)^2}{|\lambda + Z_{11}|^2} \right) \tag{6.1}$$

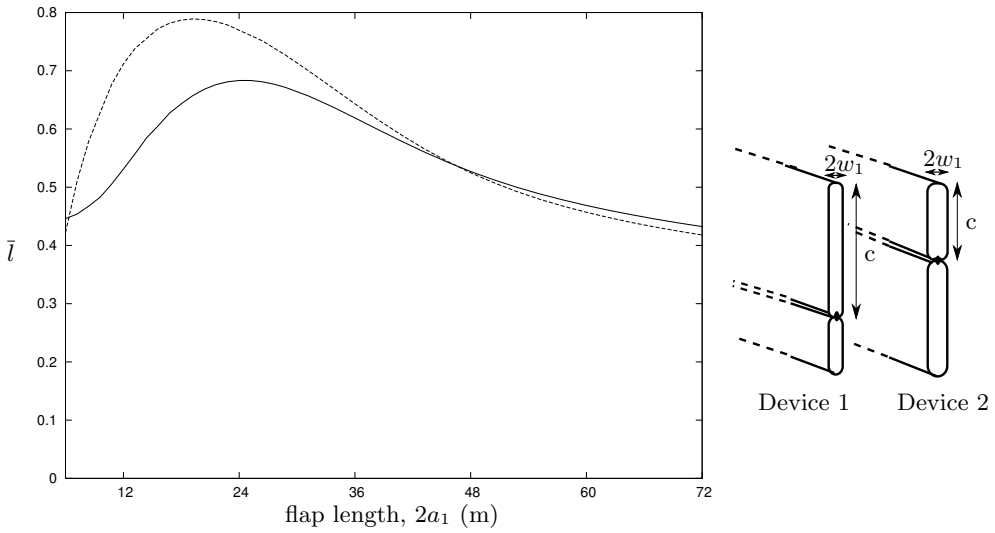

Figure 5: Variation of mean capture factor $\bar{l}$ with flap length $2a_1$ in metres along with scale diagrams of the devices. The solid line corresponds to device configuration 1 and the dashed line to device configuration 2. Optimal λ has been determined and used at each flap length.

for a single device, where

$$\hat{l}_{max} = \frac{2\pi |F_{S,1}(\beta)|^2}{2ka \int_0^{2\pi} |F_{S,1}(\theta)|^2 \, d\theta} \tag{6.2}$$

and the exciting force has been expressed as a function of incident wave direction, β, see for example Evans and Porter [7]. Thus, there are three main ingredients in the determination of the capture factor. The first (6.2) sets $\hat{l}_{max}$ and is decided by the geometry of the wave absorber. This depends on scattering of waves by the fixed absorber and is optimised by a highly directional force profile as a function of wave angle. The flap offers this feature. The second factor multiplies $\hat{l}_{max}$ to set $\hat{l}_{opt}$ and depends on hydrodynamic coefficients,

$$\frac{2\mathcal{B}_{11}}{\mathcal{B}_{11} + |Z_{11}|} = \frac{2}{1 + (1 + (\Im m\{Z_{11}\}/\mathcal{B}_{11})^2)^{1/2}}. \tag{6.3}$$

The key to optimising this is making the factor $\Im m\{Z_{11}\}/\mathcal{B}_{11}$ as small as possible over a range of periods. The final factor in (6.1) is the only point at which the controllable power take off is introduced. Here, we are looking for λ to be close to $|Z_{11}|$ over a broad range of periods. Optimising the performance of the device involves finely tuning these three components so that each is optimised in unison. An illustration of the key roles these factors play in device performance is shown in figure 4 for the optimal parameters given in table 1. We will discuss this a little later, but first we focus our attention on the numerical optimisation used to determine the optimal device configuration.

Optimal device parameters were found by taking advantage of the high numerical efficiency of the solution method to embed the calculation of the mean capture factor in a multi-dimensional numerical optimisation procedure. This was given as free parameters the flap width $2w_1$, the flap length $2a_1$, the hinge depth c, the power take-off parameter λ and the specific gravity s. Sensible bounds were set on the values these parameters could take and the depth of the water was chosen to be $h = 12m$. The optimal parameters determined are shown in table 1 along with their corresponding mean capture factors $\bar{l}$.

The first row gives optimal values when the hinge height and flap width were fixed at values representative of the Oyster [Aquamarine Power 12], termed device 1. In this case the specific gravity selects its lower bound, which was set at 0.15 whilst the optimal device length was found to be 24.6m, commensurate with the second generation 'Oyster 800' device. In the second row

Device	$2a_1$ (m)	$2w_1$ (m)	c (m)	s	λ	$\bar{l}$
1	24.6	1.9	8.4	0.15	7.54	0.684
2	19.2	2.4	5.0	0.15	2.02	0.789

Table 1: Optimal device parameters, namely length, width, hinge depth, specific gravity and power take-off parameter for a single flap are shown along with the corresponding mean capture factors. In the first row conditions particular to the Oyster device are adopted, with only $2a_1$ and λ being allowed to vary whilst in the second all parameters have been allowed to vary within sensible bounds. The depth is fixed at $h = 12$m.

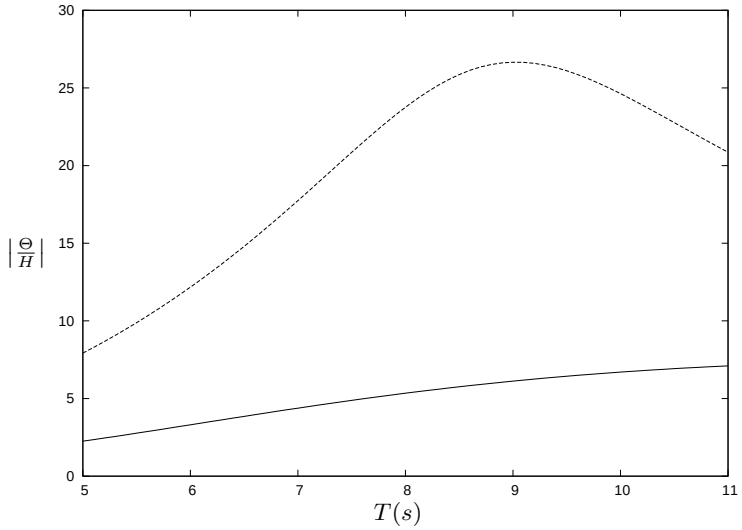

Figure 6: Maximum angle of excursion per unit height of incident wave. Results for device type 1 are shown by the solid line and results for device type 2 by the dashed line.

all parameters were allowed to vary, with the specific gravity of the flap again selecting its lower bound at $s = 0.15$. This configuration favours a shorter flap with a higher hinge point than the Oyster along with a smaller power take-off parameter. This geometry is termed device 2.

With the optimal parameters determined we return our attention to the components of optimisation shown in figure 4. First, we consider $\Im m\{Z_{11}\}/\mathcal{B}_{11}$. Resonance occurs when this quantity vanishes since when this is the case $\omega^2(\mathcal{A}_{11} + I_1) = C_1$ and the moment of inertia, plus added inertia, is balanced by the restoring forces due to buoyancy. Generally, we want it to be as small as possible across a range of periods as this results in $\hat{l}_{opt}$ remaining close to $\hat{l}_{max}$. In figure 4(a) we see one of the key features in the broad-banded success of the Oyster device; despite not achieving true resonance device 1 is near resonant across a wide range of incident wave periods. Meanwhile, in figure 4(c) we notice that the natural resonant period of device 2 does fall within the range of interest. This reduction of the resonant period is due to a combination of reducing device length, increasing the width and raising the hinge position and tallies with the numerical findings of Folley et al. [9] and Whittaker and Folley [22] where it is suggested that shorter, wider devices have lower resonant periods. Again this quantity remains small across the full range, especially for lower wave periods where the energy in the nearshore spectrum is focused.

It it through the final component that the power take-off parameter plays a part. Optimal tuning requires $\lambda = |Z_{11}|$ and results in $\hat{l}$ attaining $\hat{l}_{opt}$. Generally, λ is constant and so we are looking for $|Z_{11}|$ to be relatively flat. λ may then be fixed at a value determined by the weighted average of $|Z_{11}|$ over a real sea spectrum. Here λ has been determined to be optimal for the real sea spectrum described in §5. The explanation given above suggests mathematical reasons for the broad-banded success of flap-type converters as a wave energy design solution.

Figure 5 shows the variation of mean capture factor $\bar{l}$ with flap length $2a_1$ for both device configurations, the optimal value of λ having been determined for each length. A clear peak may

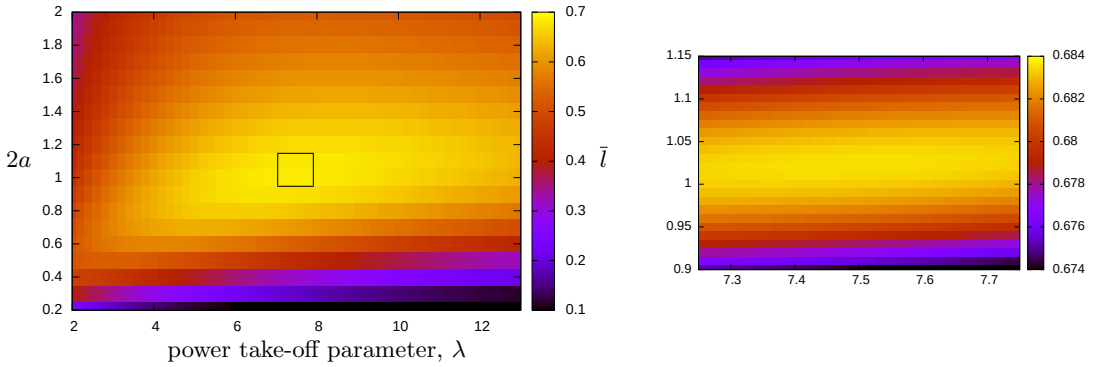

Figure 7: A heatmap showing the mean capture factor for device 1 as a function of flap length $2a$ and power take-off parameter λ. A zoomed in view of the boxed area is shown in the plot to the right.

be seen in both cases, indicating that device length is critical to performance. The peak for the second device configuration is skewed further to the left than that of device 1 suggesting a shorter optimal flap length of 19.2m when the hinge is positioned higher on the device. The maximum mean capture factor is also higher for device 2 than for device 1 demonstrating a greater power absorption potential. However, the 15% increase in $\bar{l}$ obtained with a higher hinge position is offset by a significant increase in the amplitude of the flap oscillations. In figure 6 the flap excursion per unit height of incident wave is shown as a function of incident wave period for both device 1 and device 2. The peak in the flap excursion for device 2 is suggestive of resonance at $T \simeq 9s$. The problem being that this also results in a peak flap excursion of 26.5°, motion of this magnitude is poorly approximated by a linearised theory leading to inaccurate results. Meanwhile, for device 1 (where parameters have been chosen to be representative of the Oyster) we see a maximum flap excursion per incident wave height of just 7°, confirming linearised theory is an appropriate approximation in this case. From now on we will consider only device 1, in which the hinge point is located closer to the sea bed, as this leads to smaller flap excursions and more accurate results.

Finally, figure 7 shows a heat map demonstrating the dependence of the mean capture factor on both the flap length $2a$ and the power take-off parameter, λ. Both parameters are clearly important to device performance with the marked vertical gradient in the closer view reinforcing the critical role the flap length in particular plays in device performance. It is perhaps unsurprising to note that the dependence on λ is comparatively less sensitive since in calculating the mean capture factor since an average has been taken over a spectrum of incident wave periods. Thus the advantage seen with precise tuning for single-frequency is lost.

6.2. Multiple Devices

The geometrical properties of the flaps could mathematically be allowed to vary from one device to the next, but here we have chosen to define them identically for all flaps for the sake of mathematical simplicity and since this might reflect a realistic design process. Correspondingly, for the purpose of the results presented here we will fix $a_1 = a_2 = ... = a_N \equiv a$ and $\lambda_1 = \lambda_2 = ... = \lambda_N \equiv \lambda$ so that all flaps have identical length $2a$ and power take-off λ. These are fixed at the optimal values determined in section §6.1 for a single device under the conditions most closely representative of the Oyster.

First, we would like to convince ourselves of the accuracy of the solution method for multiple flaps. To this end we consider how the exciting torque varies with separation for two identical in-line flaps. By symmetry both experience the same exciting torque, $|\hat{F}_{S,1}| = |\hat{F}_{S,2}| = |\hat{F}_S|$. Figure 8 shows $|\hat{F}_S|$ plotted as a function of $s/a = (d_2 - d_1 - 2a)/a$, the dimensionless distance between the flaps, for normal incidence, fixed $kh = 0.8$ and $a/h = 1$. As the separation increases, becoming large compared with both the incident wavelength and the device length, forces converge to those

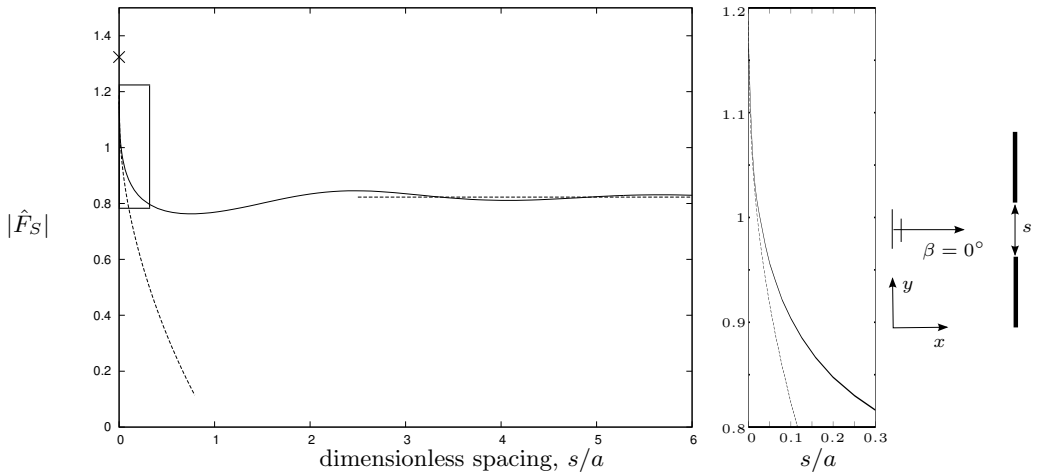

Figure 8: Modulus of the dimensionless exciting torque induced on one of two in-line flaps as a function of s/a, the spacing between them non-dimensionalised by device length, for normal incidence and fixed $kh = 0.8$. The cross shows the force induced on a single flap of twice the length whilst the dashed lines shows asymptotic limits for both small and large separations. An enlargement of the boxed area is shown to the right of the plot along with a plan view of the device set up.

for flaps in isolation. Meanwhile, as the separation becomes small the behaviour is more subtle. Here results don't converge to a single device of twice the length, as if two flaps had effectively been glued together (marked by $\times$ in figure 8). Instead, the singularities at the end points of the flaps play an important role mathematically, even for small apertures, and result in a non-uniform limit. A small gap approximation, not reported in detail here, has been made using matched asymptotic expansions (e.g. Tuck [21]) in which the inner problem consists of a gap in a barrier of infinite length and the outer problem consists of a single barrier of double length with a source placed at its centre for $x > 0$ and a sink for $x < 0$. The resulting approximation is shown in figure 8 and demonstrates good agreement with the direct computations based on §4 as the spacing $s/a \to 0$. This, in addition to other numerical checks have been used to confirm the accuracy of the results for multiple flaps.

In the following we expand on the ideas which arose from the analysis of two identical devices in Appendix A to consider optimal array configuration as would be appropriate to the context of a wave farm. Embedding the calculation of mean capture factor in a numerical optimisation procedure we take the flap positions (b_n, d_n) as free parameters for $n = 1, ..., N$. To begin with we choose $N = 3$ and consider four possible configurations of an array of three devices as shown in figure 9. Here various restrictions have been imposed on the spatial parameters according to the symmetries of the different geometries; in configuration (a) we have just one free parameter, the spacing in the y-direction, whilst in configurations (b), (c) and (d) we have two free parameters, the spacings in both x and y directions. The optimal values determined for each configuration are shown in table 2.

This demonstrates the advantage of taking the devices out of line as suggested by the analysis in Appendix A. We see a 5% improvement in performance with either of configurations (b) or (c) over that for a single device operating in isolation. This shows an effective increase in power take-off from each element in the array as a result of its appropriate configuration with optimal spacings. This enhancement in performance, due to the positive interaction effects between the devices resulting in constructive interference, is limited since we have taken the average over a directional spectrum. It has been shown, see Wolgamot et al. [24], that when averaged over all incident wave directions an array of devices will be capable of exactly the same power absorption as the sum of its parts, that is the total power absorbed from each of the devices operating independently. Nonetheless, we do see a gain in the power absorption and optimal spacings have been suggested for all four array configurations with scale diagrams being shown in figure 9.

Figure 10 shows the angular excursion per unit height of incident wave and the single-frequency

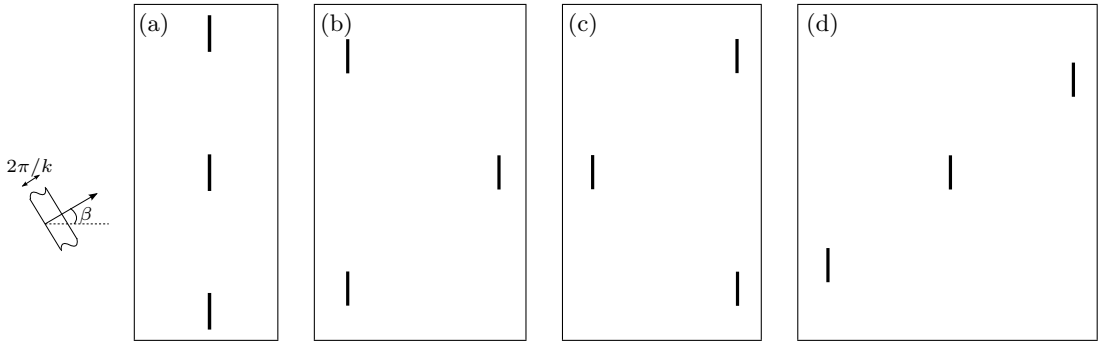

Figure 9: Plan views of configurations (a)-(d), to scale, for optimal spacings.

	Spacing (m) between devices in:		
	x-direction	y-direction	$\bar{l}$
(a)	0	43.0	0.695
(b)	51.7	40.9	0.717
(c)	51.7	40.9	0.717
(d)	50.4	37.6	0.711

Table 2: Optimal spacings in metres for four possible configurations of an array of three devices, as shown in figure 9, along with corresponding mean capture factors.

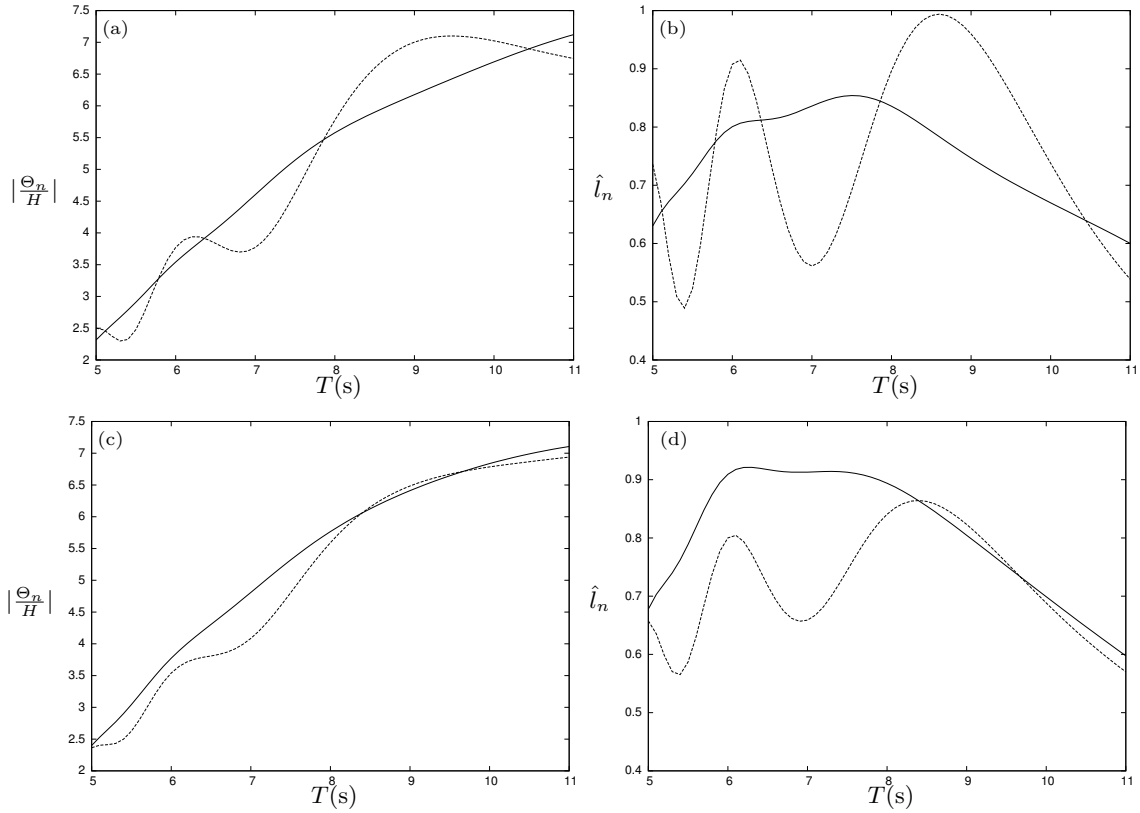

Figure 10: Variation with wave period of the angle of excursion and single-frequency capture factor in normally incident waves for each device in an array of 3 for configurations (b) and (c). Only two lines are shown in each plot due to symmetry and in all cases the solid line shows results for the fore flap(s) relative to a normally incident wave and the dashed line shows the aft flap(s).

capture factor for each device for both configurations (b) (shown in 10(a) and (b)) and configuration (c) (shown in 10(c) and (d)) subject to normally-incident waves. This example wave angle has been chosen since it corresponds to the largest system response for a symmetric array. The single-frequency capture factor on each device is defined by

$$\hat{l}_n = \frac{W_n}{2a_n W_{inc}} = \frac{1}{2}\lambda \left| \left((\mathbf{Z} + \lambda \mathbf{I})^{-1} \mathbf{F}_S \right)_n \right|^2 \tag{6.4}$$

and due to symmetry in normally incident waves we consider only two devices in each array, one fore and one aft. For both configurations we see a larger variability in capture factor and angular excursion for aft flap(s). This is especially apparent for the 'bowl'-like configuration (b) in which the single aft flap experiences a large variability in capture factor relative to the two flaps toward the fore of the configuration. For both arrangements we see the angular excursion per unit wave height remains below 7.5°, reaffirming that a linearised theory continues to make a good approximation for an array.

Next, we consider six possible configurations for an array of five devices. Again restrictions have been imposed on the spacial parameters used in the optimisation procedure according to the symmetries of the different geometries; in configuration (a) we have just one free parameter, the spacing in the y-direction, whilst in configurations (b) and (c) we have four free parameters with both a fore and aft spacing in the x-direction relative to a normally incident wave along with central and outer spacings in the y-direction. In configurations (d) and (e) we have three free parameters, the spacing in the x-direction along with both the central and outer spacings in the y-direction as before. Finally, in configuration (f) we have two free parameters, assuming the step sizes in the staggered array to be constant in size. The optimal values determined for each configuration are shown in table 3.

Here we see further improvement in the mean capture factors over both that achieved by a single device and by an array of three devices. The trend for the optimality of a symmetrical, staggered arrangement as shown in figure 11(b) and (c) continues with the larger array size, again seeing the highest mean capture factor, this time with a 7% improvement in performance over that of a single device. Meanwhile, for the in-line array with optimal spacings we see a 2% improvement in performance over a single device, whilst not being a large increase this is in the context of the possibility for deterioration in performance with less favourable spacings. The optimal spacings for all six arrangements are shown in table 3.

In figure 12 both the angular excursion per unit incident wave height and the single-frequency device capture factor are plotted as a function of wave period for arrays (b) and (c) subject to normal incidence. Here, the fore flaps are shown by the solid lines, the middle flaps by the dashed lines and the rear flaps by the dotted lines. Similar features are seen to those reported earlier for the three device arrays. Least variability in both interaction factor and angular excursion is seen for the front flaps, with increasing variation due to interaction effects for devices placed further back in the array. The angular excursion remains below 7.5° for all wave periods of interest and both configurations, again confirming linear theory to be a good approximation.

There is the possibility of considering optimal array configuration through use of the dimensionless interaction factor, q, which is defined by the ratio of maximum array power to the maximum power for a single device times the no. of devices. This is the approach which is taken in Sarkar et al. [19] where the consideration is restricted, for the most part, to normal wave incidence. However, the interaction factor is a single frequency measure and here we have favoured an approach which averages over a random wave spectrum with directional spreading. As a result the mean capture factor of both an individual device and an array has been used as a measure for performance and hence optimality.

The potential to exploit positive interaction effects to enhance the performance of each device in an array through its optimal arrangement is limited due to the spectrum of incident wave angles and periods considered. Despite this, optimal spacings have been determined for all arrangements and in every case an improvement in the mean capture factor has been achieved. The advantages of this improvement are compounded by the possibility for deterioration in performance with less favourable spacings. In fact, in Sarkar et al. [19] a deterioration of performance was seen for all array configurations in random seas, with an average interaction factor, q, of less than one. This is despite consideration of an array of thirteen devices subject to normally incident waves, where

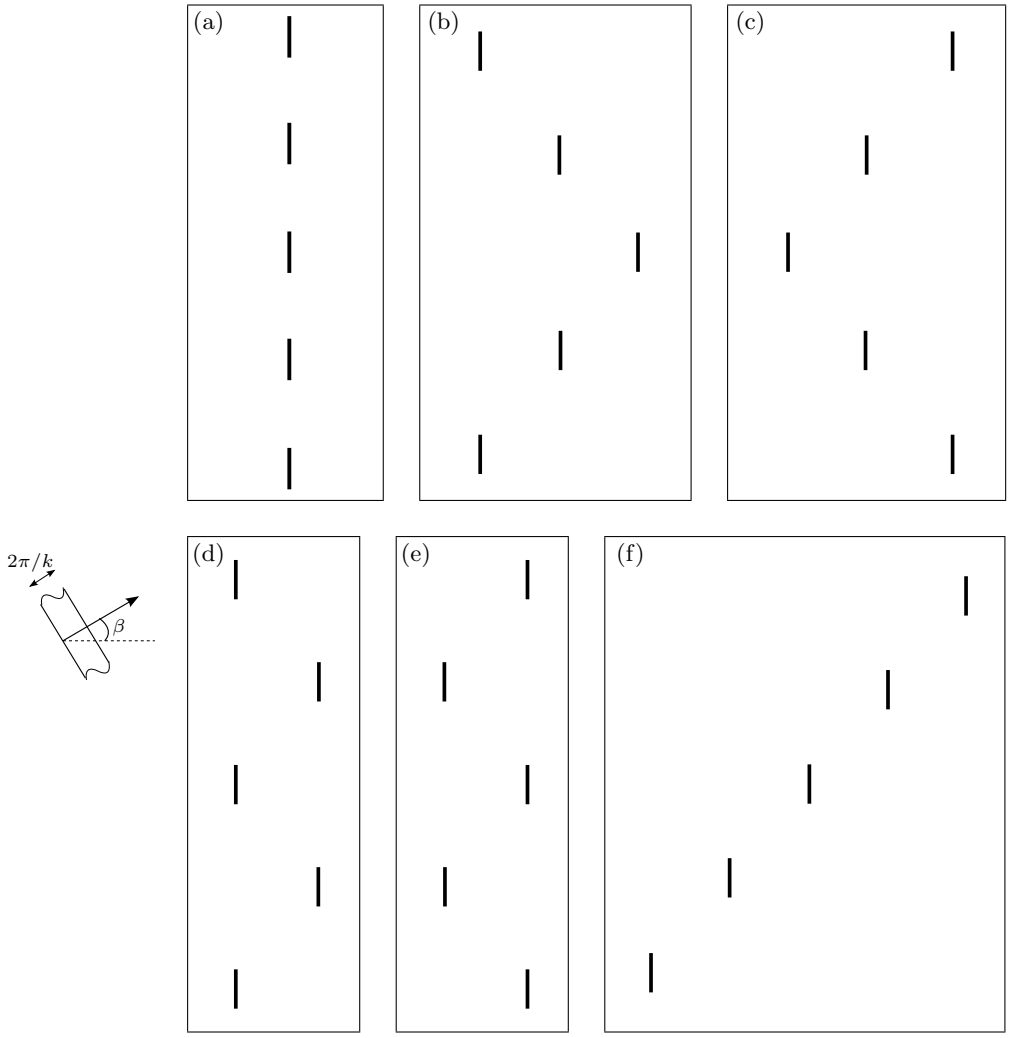

Figure 11: Plan views of configurations (a)-(f) to scale for optimal spacings.

	Spacings (m) between devices in:				$\bar{l}$
	x-direction		y-direction		
	fore	aft	central	outer	
(a)	0	0	43.9	0	0.700
(b)	49.3	52.5	39.1	37.5	0.729
(c)	49.6	51.5	38.0	38.6	0.728
(d)	51.5	0	41.1	40.8	0.727
(e)	51.5	0	41.1	40.8	0.726
(f)	50.9	0	36.0	0	0.722

Table 3: Optimal spacings, in metres, for six different configurations, shown in figure 11, of an array of five devices with corresponding mean capture factors.

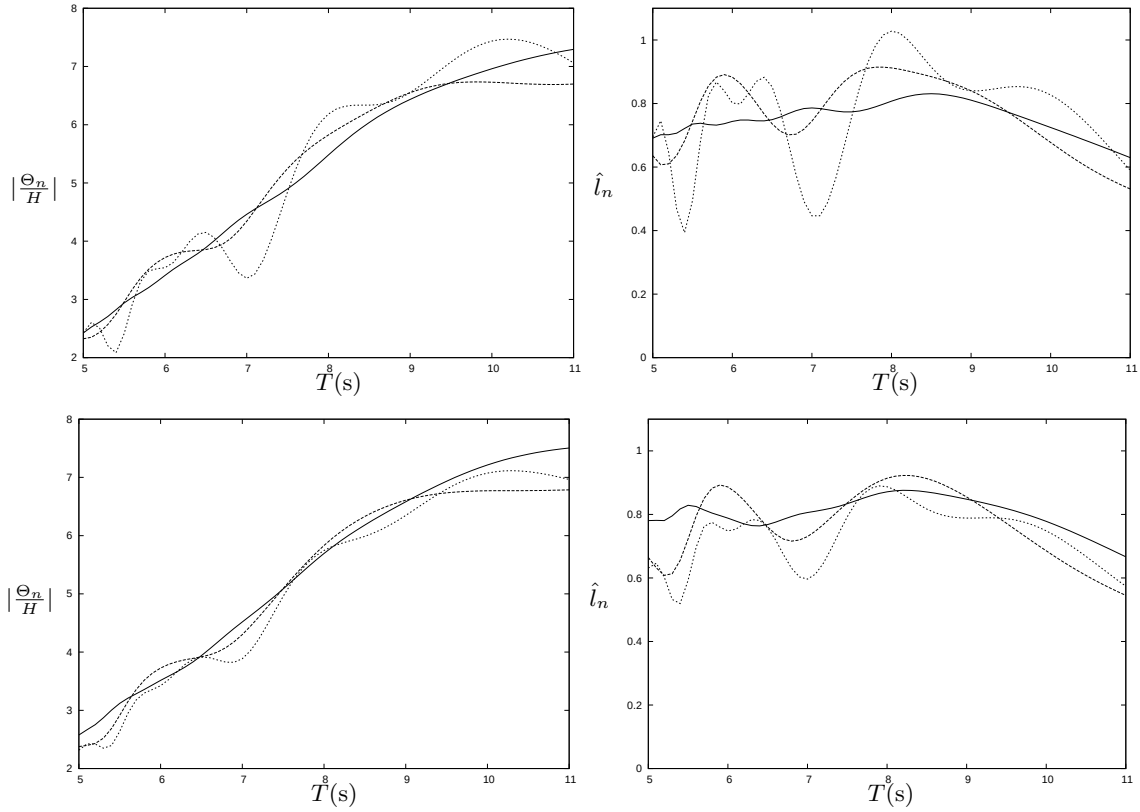

Figure 12: Variation with wave period of the angle of excursion and single-frequency capture factor of an array of 5 devices subject to normally incident waves. Results are shown for arrangement (b) in plots (a) and (b) and for arrangement (c) in plots (c) and (d). The solid lines shows results for the front flap(s), the dashed line show the mid flaps and the dotted lines the rear flap(s).

the potential to harness positive interaction effects is greater. The reason for this poor array performance is due to sub optimal spacings having been chosen for the considered spectrum. In all cases the optimal spacings are found to be well beyond the fixed spacings considered in Sarkar et al. [19].

In addition to key differences in the approach we note agreement with some of the key features observed in Sarkar et al. [19] for normal wave incidence. In particular, an enhancement of the performance of the central flap for a 'chevron' configuration is illustrated in figures 10 (d) and 12 (d) for arrays of three and five devices respectively. This agrees with observations made for a similar array shape in Sarkar et al. [19]. However, since this feature is less pronounced in obliquely-incident waves and is balanced by a less exceptional performance of other devices in the array, no clear gain in net power output is seen relative to the inverse configuration which is 'bowl'-like in shape. Further, the critical role lateral spacing plays in optimal array performance is independently identified in both papers.

7. Conclusions

In this paper, an analytical approach has been taken to calculations assessing the performance of a three-dimensional flap-type wave energy converter functioning both in isolation and within an array. The novel semi-analytic solution method developed for the treatment of this problem results in a solution which is fast, accurate and simple to implement. Advantage has been taken of the high numerical efficiency to embed the calculation of mean capture factor in an optimisation procedure. This has been used to suggest optimal flap parameters for an individual device subject to a real sea spectrum of incident wave periods and directions. The results presented appear to

align with those used by Whittaker and Folley [22] in the design process of the Oyster device. In particular, the flap length seems to be a critical factor in determining device performance with an optimal value of 24.6m being suggested. This is close to the 26m length of the second generation 'Oyster 800' device. Based on optimal flap parameters for a single device further optimisation for an array results in optimal spacings being suggested for a range of practical configurations and ultimately the proposal of an optimal arrangement for arrays of both 3 and 5 devices. It is found that by staggering the devices, allowing for greater interaction between them, an improvement in performance is seen. This, along with a preference for symmetry which is inherent to the system, results in the largest effective increase in power absorbed by the single elements being seen when the devices are arranged in either a 'bowl'-like or a 'chevron' configuration. This applies for both of the small array sizes considered of 3 and 5 devices and is indicative of a broader pattern of behaviour.

In addition to the results seen for this particular problem, the solution method could be readily adapted to other problems, for example the scattering of waves by an infinite thin barrier with a finite number of gaps; see [11]. In particular, this work is currently being extended to consider flaps which do not penetrate the entire depth. The hope being that as much power may be extracted without encountering the adverse conditions of the surface region.

Acknowledgement

I.F. Noad wishes to acknowledge the receipt of a University of Bristol Postgraduate Research Scholarship.

References

[1] Bouws, E., Günther, H., Rosenthal, W., and Vincent, C. L. (1985). Similarity of the wind wave spectrum in finite depth water: 1. spectral form. *Journal of Geophysical Research: Oceans (1978–2012)*, 90(C1):975–986.

[2] Bretschneider, C. L. (1959). Wave variability and wave spectra for wind-generated gravity waves. Technical report, DTIC Document.

[3] Carr, J. H. and Stelzriede, M. E. (1952). Diffraction of water waves by breakwaters. In *Gravity Waves*, volume 1, page 109.

[4] Cruz, J. (2008). Ocean wave energy. *UK: Springer Series in Green Energy and Technology*.

[5] Evans, D., Jeffrey, D., Salter, S., and Taylor, J. (1979). Submerged cylinder wave energy device: theory and experiment. *Applied Ocean Research*, 1(1):3–12.

[6] Evans, D. V. (1982). Wave-power absorption by systems of oscillating surface pressure distributions. *Journal of Fluid Mechanics*, 114:481–499.

[7] Evans, D. V. and Porter, R. (2012). Wave energy extraction by coupled resonant absorbers. *Philosophical Transactions of the Royal Society A: Mathematical, Physical and Engineering Sciences*, 370(1959):315–344.

[8] Falnes, J. (2007). A review of wave-energy extraction. *Marine Structures*, 20(4):185–201.

[9] Folley, M., Whittaker, T., and Van't Hoff, J. (2007). The design of small seabed-mounted bottom-hinged wave energy converters. In *Proceedings of the 7th European Wave and Tidal Energy Conference, Porto, Portugal*.

[10] Gradshteyn, I. S. and Ryzhik, I. M. (1981). *Table of integrals, series and Products*. Academic Press, 111 Fifth Avenue, New York, New York 10003.

[11] Linton, C. M. and McIver, P. (2001). *Handbook of mathematical techniques for wave/structure interactions*. CRC Press.

[12] LTD, A. P. (2014). http://www.aquamarinepower.com/. Accessed: April 2014.

[13] Morse, P. M. and Rubenstein, P. J. (1938). The diffraction of waves by ribbons and by slits. *Physical Review*, 54(11):895.

[14] Porter, R. and Evans, D. V. (1996). Wave scattering by periodic arrays of breakwaters. *Wave Motion*, 23(2):95–120.

[15] Renzi, E., Abdolali, A., Bellotti, G., and Dias, F. (2014). Wave-power absorption from a finite array of oscillating wave surge converters. *Renewable Energy*, 63:55–68.

[16] Renzi, E. and Dias, F. (2013a). Hydrodynamics of the oscillating wave surge converter in the open ocean. *European Journal of Mechanics-B/Fluids*, 41:1–10.

[17] Renzi, E. and Dias, F. (2013b). Relations for a periodic array of flap-type wave energy converters. *Applied Ocean Research*, 39:31–39.

[18] Salter, S., Jeffery, D., and Taylor, J. (1976). The architecture of nodding duck wave power generators. *The Naval Architect*, 1:21–24.

[19] Sarkar, D., Renzi, E., and Dias, F. (2014). Wave farm modelling of oscillating wave surge converters. *Proceedings of the Royal Society A: Mathematical, Physical and Engineering Science*, 470(2167):20140118.

[20] Thomas, G. (2008). The theory behind the conversion of ocean wave energy: a review. In *Ocean wave energy*, pages 41–91. Springer.

[21] Tuck, E. O. (1971). Transmission of water waves through small apertures. *Journal of Fluid Mechanics*, 49(01):65–74.

[22] Whittaker, T. and Folley, M. (2012). Nearshore oscillating wave surge converters and the development of oyster. *Philosophical Transactions of the Royal Society A: Mathematical, Physical and Engineering Sciences*, 370(1959):345–364.

[23] Williams, A. N. and Crull, W. W. (1993). Wave diffraction by array of thin-screen breakwaters. *Journal of waterway, port, coastal, and ocean engineering*, 119(6):606–617.

[24] Wolgamot, H. A., Taylor, P. H., and Eatock Taylor, R. (2012). The interaction factor and directionality in wave energy arrays. *Ocean Engineering*, 47:65–73.

AppendixA. Power take-off expressions

In this Appendix we consider strategies for determining optimal $\mathbf{\Lambda}$ for practical power take-off systems applied to arrays of wave energy devices. We begin by considering two particular forms for the power take-off matrix $\mathbf{\Lambda}$. Firstly, if $\mathbf{\Lambda} = \mathrm{diag}\left(\lambda_1, \lambda_2, ..., \lambda_N\right)$ is a real, diagonal matrix, then

$$W = \frac{1}{2}\Re e\left\{\mathbf{F}_S^\dagger \left(\mathbf{Z}^\dagger + \mathbf{\Lambda}\right)^{-1} \mathbf{\Lambda} \left(\mathbf{Z} + \mathbf{\Lambda}\right)^{-1} \mathbf{F}_S\right\} \tag{A.1}$$

Differentiating w.r.t λ_i for $i = 1, 2, ..., N$, using the identity

$$\frac{d}{dx}\mathbf{A}^{-1} = -\mathbf{A}^{-1}\frac{d\mathbf{A}}{dx}\mathbf{A}^{-1} \tag{A.2}$$

for any matrix $\mathbf{A}$ whose elements depend on x, gives

$$\frac{dW}{d\lambda_i} = \frac{1}{2}\Re e\left\{\mathbf{F}_S^\dagger \left(\mathbf{Z}^\dagger + \mathbf{\Lambda}\right)^{-1} \left(\mathbf{J}^{ii} - \mathbf{J}^{ii}\left(\mathbf{Z}^\dagger + \mathbf{\Lambda}\right)^{-1} \mathbf{\Lambda} - \mathbf{\Lambda}\left(\mathbf{Z} + \mathbf{\Lambda}\right)^{-1} \mathbf{J}^{ii}\right) \left(\mathbf{Z} + \mathbf{\Lambda}\right)^{-1} \mathbf{F}_S\right\}. \tag{A.3}$$

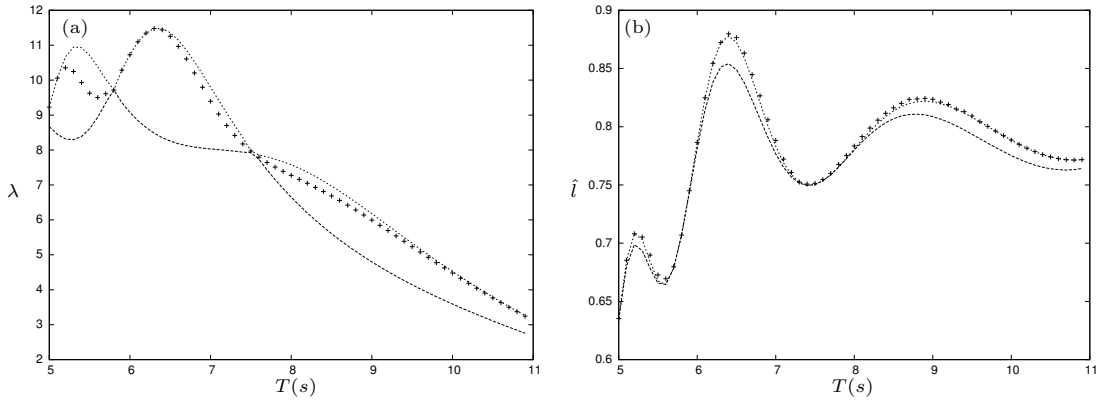

Figure A.1: Demonstration of bounds on λ_{opt}. In (a) numerical values of λ_{opt} as determined by the optimisation procedure are plotted as crosses alongside the analytic bounds $\lambda_{max} = max\{|z_1 + z_2|, |z_1 - z_2|\}$ (the dotted line) and $\lambda_{min} = min\{|z_1 + z_2|, |z_1 - z_2|\}$ (the dashed line) established in §1.3.1. These are shown for a range of incident wave periods. In (b) the capture factors corresponding to these λ are shown as a function of wave period.

Here, $\mathbf{J}^{ij}$ denotes the single entry matrix which is zero everywhere except the ijth entry which is unity. Setting (A.3) to zero for $i = 1, ..., N$ results in a system of N non-linear equations for λ_i, $i = 1, ..., N$.

Constraining $\mathbf{\Lambda}$ further so that $\lambda_1 = \lambda_2 = ... = \lambda_N \equiv \lambda$ and all devices have identical, real power take-off then the power is

$$W = \frac{1}{2}\Re e\left\{\lambda \mathbf{F}_S^\dagger \left(\mathbf{Z}^\dagger + \lambda \mathbf{I}\right)^{-1} \left(\mathbf{Z} + \lambda \mathbf{I}\right)^{-1} \mathbf{F}_S\right\} \tag{A.4}$$

which may be differentiated w.r.t λ to give

$$\frac{dW}{d\lambda} = \frac{1}{2}\Re e\left\{\mathbf{F}_S^\dagger \left(\mathbf{Z}^\dagger + \lambda \mathbf{I}\right)^{-1} \left(\mathbf{I} - \lambda\left(\mathbf{Z}^\dagger + \lambda \mathbf{I}\right)^{-1} - \lambda\left(\mathbf{Z} + \lambda \mathbf{I}\right)^{-1}\right)\left(\mathbf{Z} + \lambda \mathbf{I}\right)^{-1} \mathbf{F}_S\right\}. \tag{A.5}$$

Setting this equal to zero gives a single equation which may be used to determine the optimal value for λ. In general this must be done numerically. However, further analytic progress can be made if we assume the two flaps are identical. In this case the 2×2 matrix $\mathbf{Z}$ is symmetric about both diagonals. In other words, $\mathbf{Z}$ depends on two independent parameters, $z_1 = Z_{11} = Z_{22}$ and $z_2 = Z_{12} = Z_{21}$, say. Thus we can write

$$\mathbf{Z} = \mathbf{YDY} \tag{A.6}$$

where

$$\mathbf{Y} = \frac{1}{\sqrt{2}}\begin{pmatrix} 1 & 1 \\ 1 & -1 \end{pmatrix} \qquad \text{and} \qquad \mathbf{D} = \begin{pmatrix} z_1 + z_2 & 0 \\ 0 & z_1 - z_2 \end{pmatrix} \tag{A.7}$$

whilst $\mathbf{Y} = \mathbf{Y}^{-1} = \mathbf{Y}^T$. Now (A.4) becomes

$$\begin{aligned} W &= \frac{1}{2}\Re e\left\{\lambda \mathbf{F}_S^\dagger \left(\mathbf{Y}\left(\mathbf{D}^\dagger + \lambda \mathbf{I}\right)\mathbf{Y}\right)^{-1} \left(\mathbf{Y}\left(\mathbf{D} + \lambda \mathbf{I}\right)\mathbf{Y}\right)^{-1} \mathbf{F}_S\right\} \\ &= \frac{1}{2}\Re e\left\{\lambda \mathbf{F}_S^\dagger \mathbf{Y}\left(\mathbf{D}^\dagger + \lambda \mathbf{I}\right)^{-1} \left(\mathbf{D} + \lambda \mathbf{I}\right)^{-1} \mathbf{Y}\mathbf{F}_S\right\} \\ &= \frac{A^2}{4}\left(\frac{\lambda\left|F_{S,1} + F_{S,2}\right|^2}{\left|z_1 + z_2 + \lambda\right|^2} + \frac{\lambda\left|F_{S,1} - F_{S,2}\right|^2}{\left|z_1 - z_2 + \lambda\right|^2}\right), \end{aligned} \tag{A.8}$$

where $\mathbf{F}_S^T = A\left(F_{S,1}, F_{S,2}\right)$. It follows that

$$\frac{dW}{d\lambda} = \frac{A^2}{4}\left(\frac{\left(\left|z_1 + z_2\right|^2 - \lambda^2\right)\left|F_{S,1} + F_{S,2}\right|^2}{\left|z_1 + z_2 + \lambda\right|^4} + \frac{\left(\left|z_1 - z_2\right|^2 - \lambda^2\right)\left|F_{S,1} - F_{S,2}\right|^2}{\left|z_1 - z_2 + \lambda\right|^4}\right) \tag{A.9}$$

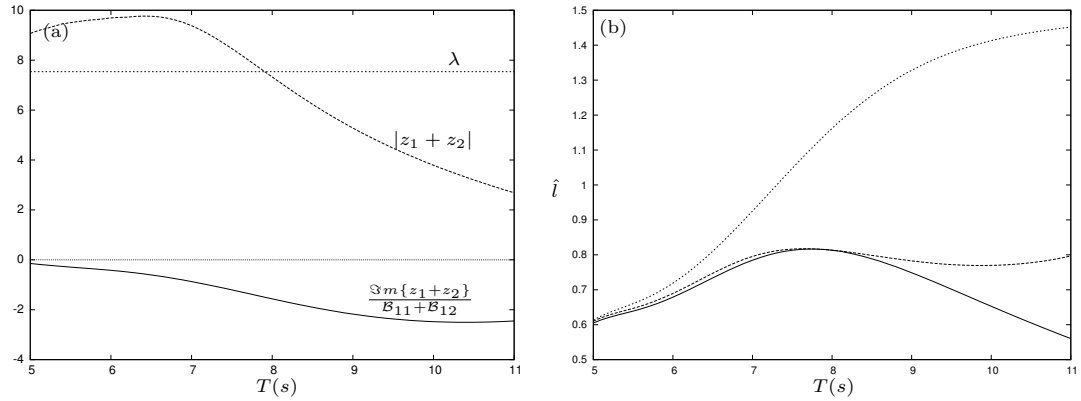

Figure A.2: Variation of: (a) $|z_1+z_2|$ and $\Im m\{z_1+z_2\}/\mathcal{B}_{11}+\mathcal{B}_{12}$, and (b) capture factors $\hat{l}_{max}$, $\hat{l}_{opt}$ and $\hat{l}$ with period T in seconds for two identical, in-line devices of type 1 (table 1) with an optimal spacing of 43.1m.

and setting this to zero determines the optimal $\lambda = \lambda_{opt}$. For this to occur, one term must be positive and the other negative and so

$$\min\{|z_1+z_2|, |z_1-z_2|\} \leq \lambda_{opt} \leq \max\{|z_1+z_2|, |z_1-z_2|\}, \tag{A.10}$$

giving bounds on the optimal power take-off parameter depending on elements of $\mathbf{Z}$. These are shown graphically in figure A.1 for two identical devices with optimal parameters as determined in §6.1 in the second row of table 1. They have been optimally positioned according to results produced using a numerical optimisation procedure with a horizontal spacing of 43.1m and a lateral spacing of 55.2m. Along with the analytic bounds, A.1 also shows optimal values for the power take-off parameter computed numerically for each wave period using the optimisation procedure of §6. These are marked by $\times$. The resulting single-frequency capture factors are shown in figure A.1(b). The values gained using analytic bounds remain within a 3% tolerance of the numerical optimum, both providing a good approximation and facilitating a faster numerical procedure by suggesting an accurate initial guess along with tight bounding conditions.

In the particular case of two identical devices, positioned in-line and subject to normally incident waves ($\beta = 0°$) then $F_{S,1} = F_{S,2}$ and we may find an exact analytic solution $\lambda_{opt} = |z_1+z_2|$. In fact, we may make an analagous decomposition to that given in (6.1) for a single device. We have

$$W = \frac{\lambda |AF|^2}{|z_1+z_2+\lambda|^2}. \tag{A.11}$$

Using the identity that $2\lambda(\Re e\{z_1+z_2\} + |z_1+z_2|) = |\lambda+z_1+z_2|^2 - (\lambda - |z_1+z_2|)^2$, for real λ, this may be rewritten as

$$W = \frac{1}{2}\frac{|AF|^2}{(|z_1+z_2|+\mathcal{B}_{11}+\mathcal{B}_{12})}\left(1 - \frac{(\lambda-|z_1+z_2|)^2}{|\lambda+z_1+z_2|^2}\right) \tag{A.12}$$

so when $\lambda = \lambda_{opt} = |z_1+z_2|$, for a specified frequency, then W may take its optimal value of

$$W = W_{opt} = \frac{2(\mathcal{B}_{11}+\mathcal{B}_{12})}{|z_1+z_2|+\mathcal{B}_{11}+\mathcal{B}_{12}}\frac{|AF|^2}{4(\mathcal{B}_{11}+\mathcal{B}_{12})}. \tag{A.13}$$

Further, if $\Im m\{z_1\} = \Im m\{z_2\} = 0$ and $\lambda = \Re e(z_1+z_2)$, or equivalently

$$I_1 + \mathcal{A}_{11} = C_1/\omega^2 \qquad \text{and} \qquad \lambda = \mathcal{B}_{11}+\mathcal{B}_{22}, \tag{A.14}$$

then the power attains its maximal value of

$$W = W_{max} = \frac{|AF|^2}{4(\mathcal{B}_{11}+\mathcal{B}_{12})}. \tag{A.15}$$

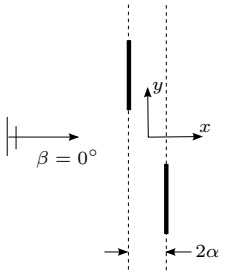

Figure A.3: Configuration of two identical, slightly out-of line flaps.

This shows that maximum power is achieved when the devices are optimally tuned at resonance; the first of (A.14) is satisfied when the inertia (including added inertia) is balanced by the restoring buoyancy torques and the second is tuneable. Figure A.1 illustrates the components of optimisation. The main difference from a single device is seen through the increase in $\hat{l}_{max}$ for the energy dense incident wave periods in the region of 6-9s. The other components of optimisation, which determine how closely the optimal and actual values lie to this theoretical maximum, take similar values to those seen before.

Meanwhile, for $\beta \neq 0$, we have $F_{S,1} = -F_{S,2}$ when $2k\,|d_2 - d_1| \sin\beta = \pi$ and $\lambda_{opt} = |z_1 - z_2|$ in this special case. Note also that $z_2 = B_{12} - i\omega A_{12} = B_{21} - i\omega A_{21}$ and so for widely separated devices $z_2 \to 0$. This implies from (A.10) that, as we would expect, $\lambda_{opt} \to |z_1|$ which is the optimal power take-off parameter for isolated devices.

Finally, we can use (A.4) to consider the effect of introducing a small offset, 2α, say to an in-line array of two identical devices under normal incidence (see figure A.3). This offset results in a phase difference of the incident wave of 2α between one flap and the next. So, to leading order, the exciting forces may be represented in the form

$$F_{S,1} = Fe^{-ik\alpha} \qquad \text{and} \qquad F_{S,2} = Fe^{ik\alpha} \tag{A.16}$$

relative to the in-line case, in which $\alpha = 0$ and $F = F_{S,1} = F_{S,2}$ denotes the exciting force exerted on either of the flaps. Substituting into the expression for the power (A.8), this gives

$$\begin{aligned} W &= A^2\lambda|F|^2 \left(\frac{\cos^2(k\alpha)}{|z_1 + z_2 + \lambda|^2} + \frac{\sin^2(k\alpha)}{|z_1 - z_2 + \lambda|^2} \right) \\ &\simeq A^2\lambda|F|^2 \left(\frac{1}{|z_1 + z_2 + \lambda|^2} + \frac{(k\alpha)^2}{|z_1 - z_2 + \lambda|^2} \right) \\ &= W_{in-line} + A^2\lambda \left| \frac{Fk\alpha}{z_1 - z_2 + \lambda} \right|^2 \end{aligned} \tag{A.17}$$

where the small angle approximations $\cos(k\alpha) \simeq 1$ and $\sin(k\alpha) \simeq k\alpha$ have been used and $W_{in-line}$ denotes the power absorbed in the in-line case. Here, (A.17) shows an immediate increase in the power absorption is achieved by taking the devices out of line. This is an effect which is seen in the main text when considering optimal array configurations where it is found numerically that staggered arrays perform the best, achieving the highest mean capture factors.